Geosci. Model Dev. Discuss., 8, 791–853, 2015
www.geosci-model-dev-discuss.net/8/791/2015/
doi:10.5194/gmdd-8-791-2015

Geoscientific Model Development Discussions
Open Access

A new chemistry option in WRF/Chem v. 3.4 for the simulation of direct and indirect aerosol effects using VBS: evaluation against IMPACT-EUCAARI data

P. Tuccella[1,2], G. Curci[1], G. A. Grell[3,4], G. Visconti[1], S. Crumeroylle[5,6], A. Schwarzenboeck[5], and A. A. Mensah[7,*]

[1]CETEMPS Centre of Excellence, Dept. Physical and Chemical Sciences, Univ. L'Aquila, L'Aquila, Italy
[2]UPMC Univ. Paris 06, Université Versailles St-Quentin, CNRS/INSU, UMR8190, LATMOS-IPSL, Paris, France
[3]Earth System Research Laboratory, National Oceanic and Atmospheric administration, Boulder, Colorado, USA
[4]2Cooperative Institute for Research in Environmental Sciences, University of Colorado at Boulder, Boulder, Colorado, USA
[5]Laboratoire de Météorologie Physique, Université Blaise Pascal, UMR 6016, Clermont-Ferrand, France
[6]LOA, UMR8518, CNRS – Université Lille1, Villeneuve d'Ascq, France

[7]Institut fur Energie und Klimaforschung: Troposphare (IEK 8), Forschungszentrum Julich GmbH, Jülich, Germany
[*]now at: Institute for Atmospheric and Climate Science (IAC), ETH Zurich, Zurich, Switzerland

Received: 8 December 2014 – Accepted: 20 January 2015 – Published: 3 February 2015

Correspondence to: P. Tuccella (paolo.tuccella@aquila.infn.it)

Published by Copernicus Publications on behalf of the European Geosciences Union.

Abstract

A parameterization for secondary organic aerosol (SOA) production based on the volatility basis set (VBS) approach has been coupled with microphysics and radiative scheme in WRF/Chem model. The new chemistry option called "RACM/MADE/VBS" was evaluated on a cloud resolving scale against ground-based and aircraft measurements collected during the IMPACT-EUCAARI campaign, and complemented with satellite data from MODIS. The day-to-day variability and the diurnal cycle of ozone (O_3) and nitrogen oxides (NO_x) at the surface is captured by the model. Surface aerosol mass of sulphate (SO_4), nitrate (NO_3), ammonium (NH_4), and organic matter (OM) is simulated with a correlation larger than 0.55. WRF/Chem captures the vertical profile of the aerosol mass in both the planetary boundary layer (PBL) and free troposphere (FT) as a function of the synoptic condition, but the model does not capture the full range of the measured concentrations. Predicted OM concentration is at the lower end of the observed mass. The bias may be attributable to the missing aqueous chemistry processes of organic compounds, the uncertainties in meteorological fields, the assumption on the deposition velocity of condensable organic vapours, and the uncertainties in the anthropogenic emissions of primary organic carbon. Aerosol particle number concentration (condensation nuclei, CN) is overestimated by a factor 1.4 and 1.7 within PBL and FT, respectively. Model bias is most likely attributable to the uncertainties of primary particle emissions (mostly in the PBL) and to the nucleation rate. The overestimation of simulated cloud condensation nuclei (CCN) is more contained with respect to that of CN. The CCN efficiency, which is a measure of the ability of aerosol particles to nucleate cloud droplets, is underestimated by a factor of 1.5 and 3.8 in the PBL and FT, respectively. The comparison with MODIS data shows that the model overestimates the aerosol optical thickness (AOT). The domain averages (for one day) are 0.38 ± 0.12 and 0.42 ± 0.10 for MODIS and WRF/Chem data, respectively. Cloud water path (CWP) is overestimated on average by a factor of 1.7, whereas modelled cloud optical thickness (COT) agrees with observations within 10 %. In a sen-

GMDD
8, 791–853, 2015

sitivity test where the SOA was not included, simulated CWP is reduced by 40 %, and its distribution function shifts toward lower values with respect to the reference run with SOA. The sensitivity test exhibits also 10 % more optically thin clouds (COT < 40) and an average COT roughly halved. Moreover, the run with SOA shows convective clouds with an enhanced content of liquid and frozen hydrometers, and stronger updrafts and downdrafts. Considering that the previous version of WRF/Chem coupled with a modal aerosol module predicted very low SOA content (SORGAM mechanism) the new proposed option may lead to a better characterization of aerosol–cloud feedbacks.

1 Introduction

It is well recognized that aerosol particles have a fundamental role in the climate system. They directly alter the budget of the radiation that reaches the Earth surface by scattering and absorbing the incoming sunlight (Haywood and Boucher, 2000), and they indirectly affect cloud properties and precipitation patterns, because they act as cloud condensation nuclei (CCN) (Rosenfeld et al., 2008; Lohmann and Feichter, 2005). Some aerosol species as black and brown carbon or mineral dust heat the atmosphere absorbing the solar radiation. The local warming may increase the atmospheric stability, leading to a decrease in cloud cover through the so called semi-direct effect (Hansen et al., 1997). The global median radiative forcing associated to the aerosol particles is highly uncertain and it is estimated to be $-0.9\,\mathrm{W\,m^{-2}}$ within a range from -1.9 to $-0.1\,\mathrm{W\,m^{-2}}$ (Boucher et al., 2013).

Experimental evidence of the influence of aerosols on macrophysical and microphysical properties of clouds have been shown in several works (Klarke and Kapustin, 2010; Christensen and Stephen, 2011; Koren et al., 2011; Ten Hoeve et al., 2011; Li et al., 2012). Several modelling studies show that aerosol particles have a strong impact not only on the climatic spatial–temporal scale, but also at short range on the regional scale (Baklanov et al., 2013). At regional scale, online coupled mesoscale meteorology–chemistry models are useful tools to take into account aerosol feedback

GMDD
8, 791–853, 2015

effects on both meteorology and atmospheric composition (Zhang et al., 2008; Baklanov et al., 2013). WRF/Chem, which is the model used in this study, is one of such models (Grell et al., 2005). In this work we present and evaluate some developments of WRF/Chem for a better simulation of direct and indirect aerosol feedback.

The introduction of the aerosol–cloud–radiation feedback leads to non-linear chains and loops of interactions between meteorological and chemical processes that are inhomogeneous in space and time (Baklanov et al., 2013). Furthermore, the prediction of meteorological variables significantly improves when the direct and indirect aerosol effects are taken into account in numerical simulation. For example, Yang et al. (2011) found that the inclusion of aerosol feedback produces significant benefits in the simulated optical and microphysical properties of marine stratocumulus, and these improvements positively affect the simulation of the boundary layer structure and energy budget. Yu et al. (2013) reported an improvement of the simulation of shortwave and longwave cloud forcing when the aerosol feedback is added to the model.

Recent studies conducted with global models, predict an important contribution of secondary organic aerosol (SOA) to direct and indirect aerosol feedback. O'Donnell et al. (2011) calculated an annual mean direct and indirect shortwave forcing of $-0.31\,\mathrm{W\,m^{-2}}$ and $+0.23\,\mathrm{W\,m^{-2}}$, respectively. Biogenic SOA (BSOA) seems to play an important role on aerosol–cloud–radiation interaction. Scott et al. (2014) find that BSOA contribute for 4–21 % to the global annual mean of CCN and 2–5 % to global mean of cloud droplet concentration. They also attribute to BSOA a global mean indirect radiative forcing ranges from -0.12 to $+0.01\,\mathrm{W\,m^{-2}}$.

Previous studies over USA and Europe demonstrated that the "traditional" configuration of WRF/Chem (Grell et al., 2005) presents a negative bias of simulated $PM_{2.5}$ mass, mostly attributable to a scarce production of SOA (Grell at al., 2006; McKeen et al., 2007; Tuccella et al., 2012). Therefore, an updated "chemistry option" with a more sophisticated treatment of SOA, fully coupled with radiative and microphysics modules, is highly desirable. In Sect. 2 of this work, we describe the developments of WRF/Chem code carried out in order to simulate the direct and indirect effects with

GMDD
8, 791–853, 2015

the new SOA parameterization (based on the Volatility Basis Set, VBS, approach) recently implemented in the model by Ahmadov et al. (2012). In Sect. 3, we describe the measurements used to evaluate the model. In Sect. 4, we evaluate the performance of the updated model through comparison with satellite data and with meteorological and chemical constituent measurements performed in the frame of the European Integrated project on Aerosol Cloud Climate and Air quality interaction (EUCAARI) (Kulmala et al., 2011). The aim of the Sect. 5 is to address the two following questions: (1) Does the introduction of SOA particles interacting with radiation and cloud processes improve the numerical prediction of cloud fields? (2) What is the potential impact of SOA particles on cloud development? The final remarks are given in Sect. 6.

2 WRF/Chem model

2.1 Description and upgrade

A pre-release of version 3.4 of Weather Research and Forecasting model with Chemistry model (WRF/Chem) (Grell et al., 2005) has been updated in order to include a new chemistry option for simulation of direct and indirect effects with an updated parameterization for SOA production. The modifications introduced by Fast et al. (2006), Chapman et al. (2009), and Ahmadov et al. (2012) are the basis of our work. The technical details of the implementation are summarized in the Appendix A.

The gas-phase mechanism used is an updated version of the Regional Atmospheric Chemistry Mechanism (RACM) (Stockwell et al., 1997). The inorganic aerosols are treated with the Modal Aerosol Dynamics Model for Europe (MADE) (Ackermann et al., 1998). The updated parameterization for SOA production is based on the volatility basis set (VBS) approach (Ahmadov et al., 2012). MADE/VBS model has three lognormal modes: Aitken, accumulation and coarse. The species treated are the sulphate ($SO_4^=$), nitrate (NO_3^+), ammonium (NH_4^+), elemental carbon (EC), primary organic matter (POM), secondary organic aerosol (SOA, anthropogenic and biogenic), chloride

GMDD
8, 791–853, 2015

(Cl), sodium (Na), unspeciated $PM_{2.5}$ (that includes the fine fraction of sea-salt and soil dust), aerosol water, unspeciated coarse fraction of PM_{10}, soil dust and sea salt.

The implementation of aerosol–cloud–radiation interaction within RACM/MADE/VBS follows the methods described by Fast et al. (2006) and Chapman et al. (2009).We modified the WRF/Chem code by preparing the inputs for the modules devoted to calculation of the aerosol optical properties and the aerosol activation, starting from the mass of each aerosol type as predicted by new chemistry package. In the approach of Fast et al. (2006), the three modes of the lognormal distribution are divided into 8 bins, and at each chemical constituent of the aerosol mass is associated a complex refractive index. The refractive index is calculated for each bin with a volume averaging. Mie theory is used to find the scattering and absorption efficiencies. Aerosol optical thickness (AOT), single scattering albedo and asymmetry parameter calculated with the optical package developed by Barnard et al. (2010), are used as input to the radiative scheme (Goddard and RRTMG). Aerosol direct effect on longwave radiation is included following Zhao et al. (2010).

Aerosol–clouds interaction is a complex problem that involves the activation and resuspension of the aerosol particles, aqueous chemistry and wet removal. Following Chapman et al. (2009), aerosols within cloud drops are treated as “cloud borne”. Aerosols that do not activate as cloud droplets are treated as “interstitial”. In WRF/Chem the activation process is based on the parameterization developed by Abdul-Razzak et al. (2000, 2002). The number and mass concentration of the activated aerosol are calculated for each mode. Within the dissipating clouds, the droplets evaporate and the cloud borne aerosols are resuspended to the interstitial state. Cloud borne aerosols and dissolved trace gases may be modified by aqueous chemistry. In this chemistry option, cloud chemistry is modelled using the scheme of Walcek and Taylor (1986). Wet deposition of trace gases and aerosols is treated in and below clouds. Within clouds the aerosols and trace gases dissolved in the water are collected by rain, graupel and snow. Below clouds the wet scavenging by precipitation is parameterized using the approach of Easter et al. (2004).

GMDD
8, 791–853, 2015

The simulation of the activation, resuspension and wet scavenging of the aerosol particles requires a prognostic treatment of the cloud droplets. The prognostic treatment of the clouds droplet takes into account the losses due to collision, coalescence, collection and evaporation, and the source due to nucleation. There are two microphysical schemes in WRF/Chem version 3.4 that include the prognostic treatment of the cloud droplet number "Lin" and "Morrison". The source due to nucleation is parameterized following Ghan et al. (1997). Both microphysical schemes take into account the autoconversion of cloud drops to rain dependent on the cloud droplet number. Therefore, aerosol activation affects both the rain rate and the liquid water content. The droplet number affects the calculation of the effective radius and cloud optical thickness (COT). The interaction of clouds with the incoming shortwave radiation is done by linking the microphysics to the radiation scheme.

2.2 Model configuration

The simulations were conducted over three 1-way nested domains centred on the Netherlands, as shown in Fig. 1. The coarse domain (D1) has 30 km horizontal resolution, domain 2 (D2) 10 km, and domain 3 (D3) is cloud resolving at 2 km resolution. In our runs we used 67 vertical levels extending up to 50 hPa.

The main physical and chemical parameterizations used are listed in the Table 1. The model setup is the same for all three domains, except that no cumulus parameterization is used for D3. Wet scavenging and cloud chemistry from both parameterized updraft and resolved clouds are taken into account in D1 and D2. However in these domains the sub-grid cloud processes involve only the interstitial aerosol, i.e. the aerosol–cloud coupling is not considered in convective parameterization. Therefore, the indirect effects are well resolved for domains with resolution less than 10 km in the version of WRF/Chem used in this work.

We simulated the period from 14 to 30 May 2008. The initial and boundary meteorological conditions for D1 are provided by the European Centre for Medium range Weather Forecast (ECMWF) analyses with a horizontal resolution of 0.5° every 6 h.

GMDD
8, 791–853, 2015

The chemical boundary conditions of D1 are taken from output of the global Model for Ozone and Related Chemical Tracers (MOZART) (Emmons et al., 2010). MOZART output has been converted to RACM/MADE/SOA-VBS species by using the "mozbc" interface that may be downloaded from the www.acd.ucar.edu/wrf-chem website.

The simulations are carried out at 24 h time-slots, starting at 00:00 UTC of each day and then run for 30 h, with first 6 h discarded as model spin-up. Meteorology of D1 is reinitialized from global analysis, while initial and boundary meteorology conditions for D2 and D3 are taken from D1 and D2, respectively. For all three domains, the chemical initial state is restarted from previous run, while the chemical boundary conditions of D2 and D3 are taken from D1 and D2, respectively. The first 13 days of May 2008 are also simulated to spin-up chemistry.

2.3 Emissions

Anthropogenic emissions data are taken from TNO 2007 inventory (Kuenen et al., 2014). TNO is a gridded European inventory with resolution of $0.125^{\circ} \times 0.0625^{\circ}$. It provides the anthropogenic emissions of NO_x, NMVOC, NH_3, SO_2, CO, primary $PM_{2.5}$ and PM_{10}. EC and primary OC emissions are also taken from TNO database that is part of the EUCAARI project (Kulmala et al., 2011).

Horizontal and vertical interpolation, temporal disaggregation, NMVOC speciation, and aggregation of emissions into WRF/Chem species is done following Tuccella et al. (2012), with minor updates described in Curci et al. (2014a). In order to prevent spurious concentration of aerosol particles, the distribution of aerosol emissions into WRF/Chem modes is based on the low emission scenario of Elleman and Covert (2010). The 10 % of the emitted aerosol mass is attributed to Aitken mode, and the 90 % to the accumulation mode.

Biogenic emissions are calculated on line with Model of Emissions of Gases and Aerosols from Nature (MEGAN) (Guenther et al., 2006). Dust and sea salt flux are also included in the simulations.

GMDD
8, 791–853, 2015

3 Measurements

We evaluated model performances in D3 against ground and aircraft based data collected in May 2008 during the Intensive Cloud Aerosol Measurement Campaign (IMPACT) in the frame of the EUCAARI project (Kulmala et al., 2009). Model results were also evaluated against MODIS satellite data.

An overview of the synoptic conditions of May 2008 over Central Europe is given by Hamburger et al. (2011). The first 15 days of May are characterized by an anticyclonic block, while the period from 16 to 31 is dominated by westerly wind and passage of several fronts. The days from 17 to 20 May are referred as "scavenged background situation" (Mensah et al., 2012), because they are dominated by northerly wind from North Sea associated to a low aerosol mass loading, due to wet scavenging. The period starting from 23 May is dominated by long range transport of dust from Sahara desert (Roelofs et al., 2010; Begue et al., 2014).

3.1 Ground based measurements

Meteorological and aerosol ground based measurements used in this study are collected in Cabauw (the Netherlands) at CESAR observatory Cabauw (Fig. 1) CESAR observatory is a tower located at 51°57′ N, 4°54′ E, and −0.7 m a.s.l., at about 50 km south of Amsterdam. Measurements performed at CESAR observatory are typical of North-West Europe, and are representative of maritime and continental conditions depending on the wind direction (Mensah et al., 2012).

Standard meteorological variables are collected at 2, 10, 20, 40, 80, 140, and 200 m height. Besides, in this study we used the measurements of temperature and relative humidity profiles obtained with radiometer, and aerosol speciation from aerosol mass spectrometry (AMS) collected at 60 m (Mensah et al., 2012).

The model is also compared to ozone (O_3), nitrogen oxide (NO_x), nitric dioxide (NO_2), nitric oxide (NO), ammonia (NH_3), nitric acid (HNO_3), nitrous acid (HONO), and sulphur dioxide (SO_2) measurements issued by Cabauw Zijdeweg EMEP station (NL0011R).

GMDD
8, 791–853, 2015

3.2 Aircraft measurements

During May 2008, the French ATR-42 research aircraft performed 22 research flights (RF). In this work we used 14 RF to evaluate the model. They are listed in Table S1. RF50, RF55, RF56, RF57, RF58, RF61 and RF62 were conducted around Cabauw supersite, in order to study the origin and characteristic of air masses collected at Cabauw. Other RFs were aimed at the study of aerosol properties along a quasi-Lagrangian flight track, with west–east and north–south transects. ATR-42 was equipped with instrumentation suitable for aerosol–cloud interaction measurements. We used the measurements from a condensation particle counters (CPC), the CPC3010 with the cutoff size of 15 nm, a Cloud Condensation Nuclei Counter (CCNC) for CCN number concentration measurements, and an AMS. A more exhaustive description of the whole campaign and instrumentation is given by Crumeyrolle et al. (2013).

3.3 Satellite measurements

The model was also evaluated with MODIS-Aqua aerosol and cloud data. The Level 2 products used here are MYD04 and MYD06 collection 051 for aerosol and clouds, respectively. For ease of comparison with model output, both satellite and model data were regridded onto a common lat-lon regular grid. Model output is sampled at same time and location of each MODIS pixel, and then data are averaged in space and time over the same grid.

4 Model evaluation

Model results are compared to ground based and aircraft observations, as detailed in Sect. 3. The statistical indices used are the Pearson's correlation coefficient (r), mean bias (MB), normalized mean bias (NMB) and normalized mean gross error (NMGE). The indices are defined in the Appendix and reported in Table 2.

GMDD
8, 791–853, 2015

4.1 Meteorology

Figure 2 shows the observed and modelled time series of hourly vertical profiles of temperature and relative humidity at Cabauw supersite. WRF/Chem reproduces the day-to-day variation of temperature, before, after, and during the wet period. As shown by statistical indices, within the first 200 m, the model reproduces the temperature with a correlation of 0.93–0.95 and a mean bias of about −0.5 °C. Looking at the free troposphere, we may realize that the model underestimates the height of the 0 °C isotherm (the black line on Fig. 2a) in the first days of simulation and during wet period by about 200–300 m (i.e., the model is colder than observed by 1–1.5 °C). Whereas immediately after the passage of the cold front, the temperature rise in the simulation is slower than observed. The model performances in simulating surface temperature are consistent with other European studies (e.g., Zhang et al., 2013a; Brunner et al., 2014). For example, Brunner et al. (2014) compared several meteorology–chemistry coupled models with annual simulations at continental scale, and found that on Central Europe the predicted surface temperature shows a correlation with observations in the range of 0.95–0.98, whereas the bias ranges from −1 to 0.1 °C.

The model reproduces the vertical structure of relative humidity (Fig. 2b) over the whole period, but it has the tendency to overestimate (underestimate) the higher (lower) observed values. This behaviour is more evident during scavenging days, when the relative humidity between 1000–2000 m is overestimated on average by 40 %, but sometimes up to 60 %. Errors of this magnitude in simulating the vertical profile of RH were already found in previous works (Misenis and Zhang, 2011; Luo and Yu, 2011). Nevertheless, the model correlation and mean bias are 0.84 and +3.4 % below 1000 m of altitude, 0.50 and +13 % in the range of 1000–2000 m, 0.78 and +6.4 % between 2000–3000 m. These values are comparable with those found by Fast et al. (2014) in the comparison of WRF/Chem simulations to aircraft data. They have shown correlations in the interval of 0.49–0.70, while the bias from −7 to +0.1 %. Near the surface,

GMDD
8, 791–853, 2015

the relative humidity is simulated with a correlation of 0.87–0.92 and a positive MB of 3–4 % (+6–8 %).

The biases of the temperature and relative humidity could be due to a misrepresentation of soil (and sea) temperature and soil moisture or by misrepresentation of the clouds and rain. These two problems are tightly coupled via land surface–atmosphere interaction. The errors in the simulation of surface moisture and energy budget influences the fluxes of latent heat and moisture in the atmosphere, affecting the local circulation, convective available potential energy (CAPE), cloud formation and rain pattern (Pielke, 2001; Holt et al., 2006). Moreover, WRF/Chem tends to fail simulating the thermodynamic variables near to coastline, because the uncertainties of land use data may play an important role (Misenis and Zhang, 2010). Initial and boundary meteorological conditions may also play an important role. Bao et al. (2005) demonstrated that meteorological prediction is sensitive to input data used. They showed that varying the inputs used as initial and boundary conditions, the mean daily model bias ranges from −2.71 to −0.65 K for the temperature and from −0.81 to 0.50 g kg^{-1} for vapour water content.

In Fig. 3 we compare the time series of observed and predicted wind speed and direction at several heights of Cabauw Tower. WRF/Chem captures the diurnal trend of wind speed, but it overestimates the wind speed during night. Generally, we found the higher correlation at 10 and 200 m (0.78 and 0.76 respectively) and higher NMB between 20 and 40 m (+30–40 %). The wind direction is captured at all altitude levels of Cabauw tower, except of 18 May when WRF/Chem does not reproduce some rapid variations, most likely due to local effects. The simulation of wind direction tends to improve with height. Indeed, the correlation coefficient increases from 0.52 to 0.73 at 10 and 200 m, respectively, and the MB decreases from 27° below 40 m to 17° at 200 m. The performance in simulating the surface wind speed are consistent with those reported by Brunner et al. (2014) in Central Europe. They have shown a correlation for 10 m wind speed in the range of 0.53–0.73 and a mean bias of 1–1.8 m s^{-1}. It is well recognized that WRF tends to overestimate the wind near the surface (e.g. Misenis

GMDD
8, 791–853, 2015

and Zhang, 2010; Ngan et al., 2013; Brunner et al., 2014), but the bias of the simulated wind speed could be also explained with uncertainties in the large-scale pattern of analysis used as input. Bao et al. (2005) showed that varying the meteorological inputs, the mean daily model bias may range from -1.53 to $-0.28\,m\,s^{-1}$ and from -1.43 to $0.01\,m\,s^{-1}$ for the u and v component of the wind, respectively.

4.2 Surface gas phase and aerosol mass

Figure 4 displays the comparison between the observed and modelled hourly time series and average diurnal cycles of O_3, NO_x, NO_2, NO, NH_3, HNO_3, HONO and SO_2 near the surface.

WRF/Chem reproduces the day to day variations of O_3, capturing its decrease during scavenging period due to low photolysis rate caused by cloud presence, recovery in the following days, and a new decrease starting from 25 May. The average daily cycle is well reproduced with a morning minimum and an underestimated maximum in the afternoon. The model simulates the O_3 with a correlation of 0.72 and systematic negative mean bias of $3.4\,\mu g\,m^{-3}$. This bias is observed in the afternoon and the evening, and is most likely due to the titration in these hours caused by higher than observed model NO_x.

WRF/Chem simulates the NO_x, NO and NO_2 time series with a correlation of 0.70, 0.65, and 0.66 respectively. The timing of NO_x daily cycle is reproduced. Indeed the model captures the morning and evening peaks and diurnal minimum of NO_2. The mean bias of modelled NO_2 is $+1.25\,\mu g\,m^{-3}$ (+20 %) and occurs in the afternoon and evening hours. Moreover WRF/Chem reproduces the morning peak and diurnal decrease of NO, but the daily cycle is affected by an average positive bias of $0.28\,\mu g\,m^{-3}$, with the average morning maximum overestimated of about $2\,\mu g\,m^{-3}$ (+33 %).

Ammonia is reproduced with a correlation of 0.43. WRF/Chem underestimates the NH_3 during the scavenging days and from 28 to 31 May. The model captures the shape of NH_3 average daily cycle, but a negative bias affects the modelled concentration at

GMDD
8, 791–853, 2015

all hours. The model mean bias over the whole period is of $-4.75\,\mu g\,m^{-3}$ (−28 %). WRF/Chem reproduces the observed HNO_3 with a poor correlation. The measured mean diurnal cycle is flat, conversely the model predicts a nocturnal minimum and diurnal maximum. The origin of model bias in simulating NH_3 and HNO_3 is discussed below, together with a discussion on inorganic aerosols.

The nitrous acid concentrations are not well captured by the model and are underestimated by 95 %. This bias could be explained by the inefficiency of NO oxidation, the only important reaction known to form HONO. However the misrepresentation of NO oxidation could not explain alone the bias. Lin et al. (2014), indeed, demonstrated that the major sources of HONO are some unknown reactions that consume nitrogen oxides and hydrogen oxide radicals.

The model reproduces the measured SO_2 with a correlation of 0.48 and a positive bias of $0.68\,\mu g\,m^{-3}$ (+90 %). The overprediction is most likely attributable to anthropogenic emissions. SO_2 is emitted mainly from isolated and elevated large point sources (Fig. S1) that are immediately mixed in the model cell leading to overestimation outside of the local plume (Stern et al., 2008). This is demonstrated, for example, by the larger NMGE for SO_2 than NO_x (116 and 45 %, respectively). NO_x is emitted near the surface by traffic and domestic heating. Therefore, NO_x emissions are subjected to a stronger temporal modulation than SO_2 point sources.

The different uncertainties found for the involved species may depend on the choice of the chemical mechanism. Knote et al. (2014) compared several chemical mechanisms within a box model constrained by the same meteorological conditions and emissions, and found that the prediction of the O_3 diurnal cycle differs by less than 5 % among the different mechanisms. Larger differences were found for other species. For example, the key radicals exhibit differences up to 40 % for OH, 25 % for H_2O_2 and 100 % for NO_3 among the selected mechanisms.

Figure 5 shows the simulated and observed time series and diurnal cycle of aerosol sulphate, nitrate, ammonium, and organic matter, at CESAR observatory. WRF/Chem

GMDD
8, 791–853, 2015

simulates the measured SO_4, NO_3, NH_4 with a correlation of 0.56, 0.68, and 0.66, respectively.

WRF/Chem captures the daily variations of SO_4 and its decrease during scavenging days. The shape of diurnal cycle is also reproduced, with the nighttime minimum and diurnal maximum. The mass concentration of SO_4 is overpredicted for the whole period with a mean bias of 1.04 $\mu g\,m^{-3}$ (+90 %). The modelled SO_4 overestimation is directly attributable to the SO_2 overprediction. Another potential source of the surplus of simulated SO_4 is related to an excessive production within the clouds. Indeed, during scavenging days, the particulate sulphate is overestimated while the predicted SO_2 does not show a bias in respect to the measurements. The overestimation of SO_4, moreover, explains in part the negative bias of predicted NH_3. The excess of particle sulphate consumes too much ammonia (Meng et al., 1997).

NO_3 is reproduced with a positive bias of 1 $\mu g\,m^{-3}$ (+72 %). Looking at diurnal cycle, the modelled nitrate is on average biased high in the daytime, with a peak in the afternoon. This maximum appears to be correlated with HNO_3 maximum. Really, the HNO_3 peak is caused by evaporation of particulate nitrate formed in the upper PBL (where the conditions of lower temperature and higher relative humidity are favourable to NO_3 formation), and mixed towards the surface by vertical mixing (Curci et al., 2014a; Aan de Brugh et al., 2012). Therefore, the unrealistic afternoon peak of modelled nitric acid should result from a too rapid relaxation of aerosol-gas partitioning to thermodynamic equilibrium (Aan de Brugh et al., 2012).

The behaviour of the simulated NH_4 is related to modelled trend of NO_3. It is biased high by 0.66 $\mu g\,m^{-3}$ (+66 %). The NH_4 overestimation is related to NH_3 underprediction (Meng et al., 1997).

Organic matter is reproduced with a correlation coefficient of 0.75. WRF/Chem reproduces the right concentration during dry period, the decrease in the wet days, and following recovery. The mean bias is negative by about 0.4 $\mu g\,m^{-3}$ and it is attributable to days from 23 to 26 May. The discussion about the origins of OM bias is given in Sect. 4.3.

GMDD
8, 791–853, 2015

The results obtained here are consistent with other modelling studies over Europe (e.g., Lecœur and Signeur, 2013; Zhang et al., 2013b; Balzarini et al., 2014). For example, the results of European annual simulations of Balzarini et al. (2014) exhibited a correlation of 0.48, 0.60 and 0.56 for surface SO_4, NO_3 and NH_4, respectively. During EUCAARI campaign, Athanasopoulou et al. (2013) reported a mean correlation of surface OM with observations of 0.56 and a mean bias of $-0.5\,\mu g\,m^{-3}$, whereas Fountoukis et al. (2014) simulates the OM at Cabauw on May 2008 with a bias of $0.3\,\mu g\,m^{-3}$.

4.3 Aloft aerosol mass

The comparison of WRF/Chem to aircraft data is done interpolating the model output point by point along the flight track. Observed and modelled aircraft data are presented by using the box plots for planetary boundary layer (PBL) and free troposphere (FT). The height of the PBL was lower than 1600 m during the whole campaign (Crumeyrolle et al., 2013). Therefore, we considered for PBL and FT concentrations the data below and above 1600 m up to 3000–4000 m, respectively. This rough approximation of PBL height could affect the comparison of the model to data.

Figure 6 displays the observed and modelled box plots of the mass concentration of SO_4, NO_3, NH_4, and OM for PBL and FT. Their mean value, over the whole period examined, standard deviation, relative mass fraction, and correlation coefficients are reported in Table 3.

The average concentrations of inorganic aerosols show little absolute error (2–8 %) with respect to the observations in the PBL, while the NO_3 and NH_4 mean concentration presents a bias of +14 and +20 % ($+0.3$ and $+0.2\,\mu g\,m^{-3}$), respectively, in the FT. The mean OM mass is biased low by a factor 2 and 3 in the PBL and FT, respectively. The correlation coefficients of SO_4, NO_3, NH_4, and OM are 0.39, 0.47, 0.43, 0.67 in the PBL and 0.23, 0.44, 0.42, 0.53 in the FT. These performances are comparable with those found with WRF/Chem (but with a different chemistry package) in California by Fast et al. (2014). They reported an absolute mean bias of about 0.01–0.2, 0.03–0.6, 0.1–

GMDD
8, 791–853, 2015

0.45, 0.2–0.57 $\mu g\,m^{-3}$ and a mean correlation of 0.42, 0.45, 0.44, and 0.72 for SO_4, NO_3, NH_4, and OM, respectively.

Although the predicted aerosol mass of each species is within the range of the observed values for most of the flights used in this study (see Fig. 4), the model does not capture the full range of the measured concentrations. This assertion is made quantitative by the standard deviations reported in Table 3. The predicted standard deviations for each species are lower than observed. In the PBL, the observed and modelled standard deviations differ by 4–10 and 55 % for inorganic ions and OM, respectively. In the FT, the difference is higher than in the PBL. The model predicts standard deviations lower than 10–40 % for inorganic particles and lower than 65 % for organic matter with respect to the measurements.

For the purpose of this analysis, it is also interesting to explore how the model reproduces the relative fraction of aerosol mass species with altitude (see Table 3). WRF/Chem overpredicts the relative fraction of the SO_4 and NO_3 by few percent in the PBL and about 10 % in FT, while the relative mass of NH_4 is overestimated by 3 % along the whole profile. The relative amount of OM is underpredicted by about 20 % in both PBL and FT. The decrease of relative amount of NO_3 and increase of SO_4 with altitude is captured by the model, while the modelled relative mass of NH_4 and OM is near constant with altitude as well as in the observations.

Looking at the individual flights, it is possible to note how the model captures the aerosol mass trend as a function of the synoptic frame in both the PBL and FT, during the dry period, scavenging days, and dust period characterized by southerly wind and passage of several fronts. The FT is the layer most affected by long range transport and cloud contamination. Therefore, the relative small bias in simulating aerosol inorganic mass in FT means that the model resolves quite correctly the large scale transport and processes related to clouds.

Nevertheless, it should be noted that SO_4 is overestimated for 8 out of 14 RFs, while NO_3 and NH_4 are underpredicted for 7–8 out of 14 RF. This SO_4 overprediction is attributable to the SO_2 excess and to a potential overproduction within the cloud

GMDD
8, 791–853, 2015

chemistry scheme. The negative bias of NO_3 and NH_4 could be explained by a low NH_3 regime, that limits the formation of the ammonium-nitrate.

The simulated OM concentration is always at lower end of the observed variability. Several factors may explain this systematic bias. First of all, our simulations do not include the processing of organic compounds in aqueous chemistry. SOA may be produced in the clouds (Hallquist et al., 2009). Modelling studies suggest that the contribution of cloud chemistry to SOA budget is almost as much as the mass formed from the gas phase (Ervens et al., 2011). OM prediction is also affected by meteorological errors. Bei et al. (2012) found that the uncertainties in meteorological initial conditions have significant impact on the simulations of the peaks, horizontal distribution and temporal variation of SOA. The same authors demonstrated that the spread of the simulated peaks can reach up to 4.0 $\mu g\,m^{-3}$. Moreover, the assumption on the deposition velocity of the condensable organic vapours (COV) may play an important role in the uncertainties of SOA production. The COV deposition velocity in the version of the VBS implemented in WRF/Chem by Ahmadov et al. (2012) is proportional to the deposition velocity of the HNO_3. The proportionality constant is a tunable parameter and in this work is set to the default value of 0.25. WRF/Chem prediction of SOA mass is very sensitive to the choice of the proportionality constant (Ahmadov et al., 2012). Previous studies have shown that SOA concentration is highly sensitive to the treatment of the deposition velocity of COV (Bessagnet et al., 2010; Knote et al., 2015). Finally we note that OM bias could be partially explained by the uncertainties in the anthropogenic emissions (e.g. bias or spatial distribution) of primary organic carbon and in the factor 1.6 used to convert them to primary OM (POM) (Turpin and Lim, 2001). The reader should also consider that the uncertainties in POM simulation affect the SOA formation. Indeed, the partition between COV and SOA used in VBS approach, depends on the total OM (Ahmadov et al., 2012).

GMDD
8, 791–853, 2015

4.4 Aloft aerosol particles

The comparison of WRF/Chem output with aircraft measurements of the number concentration of condensation nuclei (CN) and of cloud condensation nuclei (CCN) at 0.2 % of supersaturation is done by using the boxplots as for aerosol mass. In this case the modelled and measured data are smoothed by using a 10 s running mean.

Figure 7 reports the comparison of observed and modelled CN within PBL and FT. The measured and predicted average, standard deviation, and correlation of CN number over the whole period of our analysis are reported in Table 3.

The model resolves the decrease of a factor 5–6 of CN concentration between the PBL and the FT. The differences in simulated concentrations between land and sea (RF51 and 52) are also captured by the modelling system. Nevertheless, WRF/Chem overestimates, on average, the observed CN by a factor 1.4 and 1.7 within PBL and FT, respectively. The bias is less pronounced above the sea during the (RF51 and RF52), where the anthropogenic sources are less important. Moreover, it should be noted that in some cases, for example during the RF56, 57 and 58, the predicted CN are completely outside the range of the observed values. In these cases the predicted CN are biased high by about a factor of 2–3. Predicted CN shows a higher variability than measured, especially in the free troposphere where the difference of modelled standard deviation is biased high by 155 %. Anyway, the model correlation with observations is 0.40 and 0.74 in PBL and FT, respectively. These values are consistent with the 0.61 found by Luo and Yu (2011).

Figure 8 shows the comparison of observed and modelled CCN. The measured and predicted average and standard deviation of CCN are showed in Table 3. The bias of simulated CCN appears more contained with respect to CN prediction, especially in the free troposphere. The major uncertainties in predicted CCN arise from aerosol nucleation rate and primary emissions (Lee et al., 2013). Direct emission of aerosol particles is the key factor for CCN production in the PBL and near particle sources (Spracklen et al., 2006), and account for 55 % of the total global production (Merikanto et al., 2009).

GMDD
8, 791–853, 2015

On the other hand, nucleation and subsequent growth up to CCN size is an important mechanism of CCN formation in many parts of the atmosphere (Sotiropoulou et al., 2006). Using several nucleation parameterizations, Pierce and Adams (2009) showed that CCN averaged within the PBL of varies by 12 %. At the same time, they also found that varying by a factor of 3 the primary emissions, the CCN mean changes by 40 % in the PBL. On the basis of these argumentations and the correlation of predicted CN larger in the FT than in PBL (i.e. far from anthropogenic sources), we may speculate that the errors in the CCN prediction arise mainly from the uncertainties in the primary emissions of the aerosol particles.

The analysis of CCN efficiency reveals other interesting features in the model behaviour. The CCN efficiency is given by CCN/CN ratio and represents the ability of aerosol particles to nucleate cloud droplets (Andrea and Rosenfeld, 2008). CCN efficiency observed during the studied RFs is in the range of 0.02–0.33 for PBL and 0.18–0.41 in the FT, while the model predicts values of 0.03–0.17 and 0.04–0.18 for PBL and FT, respectively. In other words, WRF/Chem underestimates the CCN efficiency by a factor of 1.5 and 3.8 in the PBL and FT, respectively. Moreover, the modelled CCN efficiency is almost the same in the PBL and in the FT.

The CCN efficiency should be calculated with the aerosol population with size larger than the minimum activation diameter. The latter depends on the aerosol type and ranges from about 50 to 125 nm. In this case we calculated the observed CCN/CN ratio with the measurements of CPC 3010 that gives the total number of particles larger than 15 nm, whereas modelled CCN fraction is calculated with the total particles of the three modes of the lognormal distribution. Therefore the so calculated CCN efficiency is underestimated. Indeed, the observed efficiencies during the IMPACT campaign calculated with particles larger than 100 nm are in the range of 0.28–0.4 and 0.38–0.6 in the PBL and FT (Crumeyrolle et al., 2013), respectively. However, the simulated CCN fraction calculated with the particles of the accumulation mode, is always underestimated with respect to the observations, and it is in the range of 0.17–0.3 in PBL and 0.23–0.36 in FT. The model deficiency in simulating the CCN/CN ratio could be at-

GMDD
8, 791–853, 2015

tributable to a low number of particles in the accumulation mode or to uncertainties in the hygroscopicity of aerosol particles.

4.5 Comparison with MODIS data

WRF/Chem output was also compared to aerosol optical thickness (AOT), cloud water path (CWP) and cloud optical thickness (COT) retrieved by MODIS-Aqua.

Figure 9 shows the comparison between the AOT at 550 nm measured by MODIS and the corresponding AOT predicted by the model during the high pressure period on 14 May 2008. WRF/Chem reproduces the spatial distribution of observed AOT, such as the lowest values in the southern part of the domain or the highest values around Cabauw, but underestimates the strong gradient between eastern boundary and the centre of the domain. The model overestimates the regional mean of AOT, indeed the domain averages are 0.38 ± 0.12 and 0.42 ± 0.10 for MODIS and WRF/Chem data, respectively. The overestimation may be attributable to the overprediction of the number concentration. Moreover, model intercomparison revealed that the 30–35 % of the uncertainties in simulating the AOT arises from the assumption on the mixing state, whereas only 10 % may be attributable to the choice of species density, refractive index, and hygroscopic growth factor (Curci et al., 2014b).

Modelled CWP was calculated by vertically integrating all cloud mixing ratio (water, rainwater, ice, snow and graupel). Predicted COT is given by the contribution of the liquid water and ice. The contribution of the liquid water was estimated starting from liquid water content and droplet effective radius. The contribution of ice phase to COT was calculated following Ebert and Curry (1992).

Figures 10 and 11 show the comparison between the predicted CWP and COT, and those from MODIS in two different days, during the scavenging days (17 May) and Saharan dust period (25 May), respectively. For both days, WRF/Chem reproduces several features of the cloud systems: the maximum of CWP off the Dutch coast, on the north-western and southern parts of the domain on 17 May, and the north–south

GMDD
8, 791–853, 2015

gradient of CWP on 25 May. Similar observations may be done for COT. However, it should be noted that the model tends to shift the real position of the clouds.

As shown in Table 4, the domain average of CWP is overestimated by the model by a factor of about 1.7. The CWP overprediction might be due to the overestimation of droplet number concentration. High number of droplets stems from overestimation of CN. Another reason that could explain the positive bias of modelled CWP, is the inefficient autoconversion of cloud water to rain, typical of the Morrison microphysical scheme (Saide et al., 2012). Mean COT is predicted within 10 % of the observed values. The biases found here are quite different from the WRF/Chem study by Yang et al. (2011) on the modelling of marine stratocumulus in Southeast Pacific. They have shown a bias of +30 % in reproducing the COT, while CWP was underestimated by a factor 1.3. The reader should note that in Yang et al. (2011) the aerosol model adopted is different from the one used here and SOA formation was not included at all.

Figure 12 displays the distribution functions of CWP and COT. WRF/Chem captures the shape of the distribution functions of both variables, but underestimates the maximum and overestimates the higher and lower end of the distributions. Both variables show a variability higher than the observations. The predicted standard deviations (Table 4) are about 3.5 and 1.5 times larger than those observed for CWP and COT, respectively. This probably stems from the large variability in simulated CCN.

One typical source of error in the prediction of cloud fields, are the choices related to the model setup. For example Otkin and Greenwald (2008), evaluating the response of WRF model to the permutation of several PBL and cloud microphysical schemes, found a strong sensitivity of cloud properties. Moreover, the same authors have shown that the low level clouds are sensitive to PBL parameterization, whereas the upper level clouds are sensitive to both PBL and microphysics schemes.

One element that may affect the model-satellite comparison are the uncertainties associated to the retrieval. For example, in South-Pacific stratocumulus, MODIS overestimates the droplet effective radius by 13–20 % with respect to in situ measurements

GMDD
8, 791–853, 2015

(Painemal and Zuidema, 2011; King et al., 2013). The concomitant overestimation of COT by MODIS results in the overestimation of CWP (King et al., 2013). Henrich et al. (2010) have shown systematic differences between MODIS data and in situ observations. Indeed, analysing a system of thin cumulus clouds during EUCAARI campaign, they also found that MODIS overestimates the droplet effective radius by a factor 2–3 and COT is 2–3 times lower than in situ measurements.

5 Impact of SOA particles on cloud prediction

The last part of this study focused on the evaluation of the impact of SOA on the simulation of cloud fields. We performed one simulation for 17 May without the SOA (NOSOA), and compared it to the reference run (CTRL) discussed so far. NOSOA run is carried out only in the higher resolution domain (D3). The simulation is initialized at 00:00 UTC with the same meteorological and chemical input data used for CTRL. The only difference is that the SOA concentration is set to zero. We chose the 17 May because around 06:00 UTC, a frontal system associated to a trough from North Sea crossed the Benelux area (Fig. S2).

Figure 13 displays the comparison of CWP and COT distribution functions simulated in CTRL and NOSOA. As expected, the CTRL run predicts larger CCN and droplet than the NOSOA run (Fig. S3 and S4). The lower number of CN in NOSOA leads to reduction of CWP, and its distribution function shifts toward lower values with respect to CTRL. At the same time, ticker clouds decrease in NOSOA, whereas thin clouds enhance. Clouds with low water path (CWP $< 500\,\mathrm{g\,m^{-2}}$) increase by 17 %. Therefore, NOSOA exhibits an average decrease of CWP by 40 % with respect to the reference simulation (595 and 370 $\mathrm{g\,m^{-2}}$ in CTRL and NOSOA, respectively). The COT distribution function predicted in the sensitivity test is quite different from observations. NOSOA has 10 % more optically thin clouds (COT < 40) with respect to CTRL. Thin clouds account for respectively 94 and 84 % of the total in CTRL and NOSOA, whereas they make 92 % of MODIS dataset. The average COT predicted in NOSOA is about half

GMDD
8, 791–853, 2015

that of the CTRL run (26 and 40 respectively). The decrease of cloud optical depth in NOSOA is interpretable with larger effective radius of cloud droplets due to lower droplet number. Smaller effective radius combined to less liquid water content leads to lower values of COT.

Now it is interesting to explore the impact of SOA on the vertical structure of the cloud fields. In both runs, some isolated and shallow clouds form during the night. When the cold front reaches Benelux around 05:00–06:00 UTC, a low pressure centre forms (Fig. S5). The winds rotate around the low pressure with speeds up to 14 $m\,s^{-1}$ at 925 hPa height (Fig. S6). A convective system develops around the vortex. Figure 14 shows the maximum radar reflectivity (maximum dBz) at 06:00 UTC for CTRL simulation, and the difference of maximum dBz between CTRL and NOSOA runs. In general, the echo is larger for run with SOA, i.e. the intensity of the storm is stronger in the CTRL run. Figures 15 and 16 show the vertical fields of $PM_{2.5}$ mass, vertical wind, liquid and frozen hydrometeor for both runs in the cross section A displayed in Fig. 14. These differences between both simulations (CTRL-NOSOA) within cross section A, are also displayed in Figs. 14 and 15. The convection appears to be stronger in the control simulation, with a larger amount of hydrometeors and stronger updrafts and downdrafts. The larger differences in the simulated fields of vertical wind and hydrometeors occur in the same location where occurs the enhancement of $PM_{2.5}$ mass at cloud base (950–900 hPa), roughly at the distance of 5–15 and 40–90 km away the origin of the cross section A (Figs. 14 and 15). The results should be taken with caution because the aerosol–cloud interaction is treated only for liquid clouds, the interaction of aerosol with ice phase is still missing in the model. Although the aerosol–cloud interaction is a nonlinear process, it is possible to give an interpretation of the results with the conceptual model for cloud invigoration proposed by Rosenfeld et al. (2008). The larger number of CCN in CTRL may curb the autoconversion rate of droplets to raindrops, therefore the beginning of precipitation may be delayed with respect to NOSOA. This delay leads to a larger amount of condensed water that crosses the freezing level and forms ice hydrometeors. The freezing process warms the higher layers of the cloud

GMDD
8, 791–853, 2015

through release of latent heat, whereas the melting due to falling of ice cools the lower levels. This thermodynamic disequilibrium enhances the upward transport of heat. The enhanced conversion of CAPE to kinetic energy may yield the cloud invigoration found in the CTRL simulation.

6 Summary and conclusions

Secondary organic aerosol particles play an important role in the aerosol–cloud–radiation interaction because they contribute to the global budget of radiation and cloud condensation nuclei (CCN). The introduction of SOA particles in numerical simulations has the potential to reduce the uncertainties on the prediction of meteorological fields and air quality. To this aim, a parameterization for SOA production based on the recent VBS approach was coupled with microphysics and radiative schemes in the WRF/Chem community model.

The performances of the updated model at cloud resolving scale (2 km horizontal resolution) were evaluated using ground- and aircraft-based measurements collected during the IMPACT-EUCAARI campaign and the data from the MODIS satellite instrument. The study focuses on the Benelux area, around the supersite of Cabauw, from 14 to 30 May 2008. The analyzed period was characterized by few days of high pressure (14–15 May), followed by a scavenged background situation (17–20 May), and finally by long range transport of Saharan dust with the passage of southerly fronts (23–31 May).

The model reproduces the variations of meteorological variables as a function of the synoptic frame. The model broadly captures the inter- and infra-diurnal variability of O_3 and NO_x at the surface. The concentration of NH_3 is underestimated. Concentrations of HNO_3 and HONO is reproduced with poor correlation. Simulated SO_2 shows a positive bias of +90 %, probably due to overestimated point sources. Surface aerosol mass of SO_4, NO_3, NH_4, and OM is simulated with a correlation larger than 0.55. Their diurnal variations as a function of the synoptic frame are resolved by the model. The

GMDD
8, 791–853, 2015

bias of simulated inorganic aerosol mass is explainable together with error of SO_2, NH_3, and HNO_3 in terms of anthropogenic emissions and the approximation to instantaneous thermodynamic equilibrium. The performances in reproducing the surface aerosol mass found here are comparable to other European studies where these variables are simulated with correlations range from 0.5–0.7 (e.g., Lecœur and Signeur, 2013; Zhang et al., 2013b; Balzarini et al., 2014, for inorganic species; Athanasopoulou et al., 2013; Fountoukis et al., 2014; Li et al., 2013; Knote et al., 2011, for organic aerosols).

The analysis of aircraft data reveals that WRF/Chem captures the aerosol mass trend both in the PBL and the free troposphere (FT). The predicted aloft aerosol mass of each species is within the range of the observed values, but the model does not capture the full range of the measured concentrations: the modelled standard deviations of aerosol mass are lower than those observed. Nevertheless, SO_4 (NO_3 and NH_4) mass is overpredicted (underpredicted) in more than half of the flights. SO_4 bias is attributable to the SO_2 excess and to a potential overproduction within the cloud chemistry scheme. The negative bias of NO_3 and NH_4 could be explained by a low concentration of NH_3 that limits the formation of the ammonium-nitrate. The simulated OM concentration is at lower end of the observed mass. The bias is attributable to the missing aqueous chemistry processes of organic compounds, uncertainties in meteorological fields, assumption on the deposition velocity of condensable organic vapour, uncertainties in the anthropogenic emissions of primary organic carbon, and in the factor (1.6) used to convert them to POM. In general, the statistical analysis reveals that the predicted average concentrations of inorganic aerosols show absolute error of 2–8 % in the PBL, while the NO_3 and NH_4 are simulated with a bias of +14 % and +20 % (+0.3 and +0.2 $\mu g\,m^{-3}$), respectively, in the FT. The mean OM mass is underestimated by a factor 2 and 3 in the PBL and FT, respectively. These bias are similar to those reported by Fast et al. (2014) comparing WRF/Chem (but with a different chemistry package) to aircraft data issued in California. Indeed they found an absolute mean bias

GMDD
8, 791–853, 2015

of about 0.01–0.2, 0.03–0.6, 0.1–0.45, 0.2–0.57 $\mu g\,m^{-3}$ for SO_4, NO_3, NH_4, and OM, respectively.

Condensation nuclei (CN) are overestimated by a factor of 1.4 and 1.7 in the PBL and FT, respectively. However, in some cases, the predicted CN are overestimated by a factor of 3. Predicted CN show higher variability than measurements. The model correlation with observed CN is 0.40 and 0.74 in PBL and FT, respectively. These values are consistent with the 0.61 below 10 km of altitude found by Luo and Yu (2011). Model biases in predicting CN are attributable in large part to the uncertainties of primary particle emissions (mostly in the PBL) and to the nucleation rate.

The bias of simulated CCN is more contained with respect to that of CN. The CCN efficiency (CCN/CN ratio) is underestimated by a factor of 1.5 and 3.8 in the PBL and FT, respectively. This could be due to a low number of particles in the accumulation mode or to uncertainties in the hygroscopicity of aerosol particles. CCN/CN ratio represents the ability of aerosol particles to nucleate cloud droplets. Therefore, its misrepresentation may lead to issues in the simulation of cloud droplet number. In other words, the uncertainties in CCN efficiency is a general modelling problem that may prevent a correct representation of the amplitude of the aerosol–cloud interaction, i.e. the response of microphysical cloud properties to the variation of CCN load. This issue surely deserves and warrants further insight in the future.

The bias of simulated CN affects the prediction of aerosol optical thickness (AOT), cloud water path (CWP), and cloud optical thickness (COT). The comparison with MODIS data shows that the model overestimates the AOT. The AOT averaged over the entire domain on a single day are 0.38 ± 0.12 and 0.42 ± 0.10 for MODIS and WRF/Chem data, respectively. CWP is overestimated by a factor of 1.7, whereas modelled COT agrees with observation within 10 %. The overprediction of CWP could be due to the overestimation of droplet number concentration that results from the overestimation of CN, and to inefficient autoconversion of cloud water to rain. The reader should note that the model error found here are different from the study conducted with WRF/Chem by Yang et al. (2011) on the modelling of marine stratocumulus in South-

GMDD
8, 791–853, 2015

east Pacific where SOA formation was not included in the simulations. Those authors reported a bias of +30 % in reproducing the COT, while CWP was underestimated by a factor 1.3

As test application of the new chemistry option, we performed a sensitivity simulation where the SOA particles are excluded. The aim was to answer to two questions:

1. Does the introduction of SOA particles improve the numerical prediction of cloud fields?

   The introduction of the SOA in the numerical simulation, as shown in Fig. 13, improves the prediction of CWP only for values less than 50 g m^{-2}. The lower number of CN in sensitivity simulation reduces the CWP, and its distribution function shifts toward lower values with respect to the reference run. The decrease of CWP is of about 40 %. However, cloud microphysics scheme used in this study (Morrison) presents an inefficient autoconversion of cloud water to rain (Saide et al., 2012) that leads to overestimation of the CWP in the control run. Therefore, the use of a scheme with a more reliable conversion from cloud water to rain, could underestimate the observed CWP in a simulation without SOA while could give values closer to the measurements when including SOA.

   Conversely to CWP, COT prediction is much improved by introduction of SOA. The sensitivity test exhibits 12 % more optically thin clouds (COT < 40) with respect to the reference simulation. The thin clouds are respectively 82 and 94 % of the total in control and sensitivity run, whereas they make about 97 % in the MODIS dataset. The average COT predicted in the run without SOA is 26, 41 in the control run, and 38 in the observations.

2. What is the impact of SOA particles on cloud development?

   The analysis was conducted on a convective system. The simulated radar reflectivity is larger for run with SOA, i.e. the intensity of the storm is stronger in the control run. The control simulation exhibits a larger amount of hydrometeors and stronger updrafts and downdrafts. The larger differences in the simulated fields of

GMDD
8, 791–853, 2015

vertical wind and hydrometeors occur in correspondence of the larger differences in the of $PM_{2.5}$ mass at the cloud base.

On the basis of the results discussed in the work, the option RACM/MADE/VBS coupled with cloud microphysics and radiation allows the WRF/Chem community to use a powerful tool for the study of the aerosol–cloud interactions, improved in terms of representation of the aerosol processes with respect the previous versions based on the RADM/MADE/SORGAM scheme.

For the future there is still large space for improvements. For example, a more advanced treatment of deposition of condensable organic vapors is desirable. Moreover, the missing production of SOA in cloud is a gap that should also be filled. Finally, the extension of aerosol–cloud interaction to the ice-phase would lead to a complete representation of the aerosol indirect effects.

Appendix A: Technical details of coupling of VBS scheme with radiation and microphysics schemes

The new chemistry option in namelist.input is *chem_opt* = *44*. It works with both *Lin* and *Morrison* microphysics scheme, *Goddard* and *RRTM* shortwave scheme, and *RRTM* longwave parameterization. Coupling of new scheme for SOA production with microphysics and radiative processes requires several modifications to code:

1. The first step is to create a new chemistry option. The package racm_soa_vbs_aqchem_kpp (chemopt == 44) has been added to/Registry/registry.chem together to some new model variables for the cloud-borne organic aerosols, called, for example, *asoa1cwi*, *asoa1cwj* etc.

2. New chemistry package is a KPP option. Therefore, we created a new subdirectory in */chem/KPP/mechanisms/racm_soa_vbs_aqchem* containing the files (*.spc, *.eqn, *.kpp, and *.def) where are defined the chemical model species

GMDD
8, 791–853, 2015

and constants, chemical reactions in KPP format, model description, computer language, precision and integrator. The files are the same used in *racm_soa_vbs_kpp* package (chemopt == 108).

3. The last step is to update the subroutines in *chem* subdirectory. In order to call necessary subroutines, the modules that we modified are:
   - *chemics_init.F*
   - *module_input_chem_data.F*
   - *mechanism_driver.F*
   - *cloudchem_driver.F*
   - *module_sorgam_aqchem.F*
   - *module_wetscav_driver.F*
   - *module_aerosols_soa_vbs.F*
   - *aerosol_driver.F*
   - *dry_dep_driver.F*
   - *module_mixactivate_wrappers.F*
   - *emissions_driver.F*
   - *module_bioemi_megan2.F*
   - *optical_driver.F*
   - *module_optical_averaging.F*
   - *module_ctrans_grell.F*

Appendix B: Statistical indices used in the model evaluation

Let Obs_i and Mod_i be the observed and modeled values at time i, and N the number of observations.

GMDD
8, 791–853, 2015

– The Pearson's Correlation (r):

$$r = \frac{1}{N}\sum_{i=1}^{N} Z_i(\mathrm{Mod}) \cdot Z_i(\mathrm{Obs})$$

$$Z(\boldsymbol{X}) = \frac{\boldsymbol{X} - \langle \boldsymbol{X} \rangle}{\sigma_{\boldsymbol{X}}}$$

where $\boldsymbol{X}$ is a generic vector, $Z(\boldsymbol{X})$ is its standard score, and $\sigma_{\boldsymbol{X}}$ is the SD.

– Mean Bias:

$$\mathrm{MB} = \frac{1}{N}\left(\sum_{i=1}^{N} \mathrm{Mod}_i - \mathrm{Obs}_i\right)$$

– Normalized Mean Bias (NMB):

$$\mathrm{NMB} = \frac{1}{N}\sum_{i=1}^{N} \frac{\mathrm{Mod}_i - \mathrm{Obs}_i}{\mathrm{Obs}_i} \times 100$$

– Normalized Mean Gross Error (NMGE):

$$\mathrm{NMGE} = \frac{1}{N}\sum_{i=1}^{N} \frac{|\mathrm{Mod}_i - \mathrm{Obs}_i|}{\mathrm{Obs}_i} \times 100$$

GMDD
8, 791–853, 2015

Code availability

The code updated, described, and evaluated here will be incorporated in the next version (3.7) of WRF/Chem, which will be released to the user's community in spring 2015. The users will be able to freely download the code from the WRF website (http://www2.mmm.ucar.edu/wrf/users/download/get_source.html). A general WRF/Chem user's guide is also available online (http://ruc.noaa.gov/wrf/WG11/).

The Supplement related to this article is available online at doi:10.5194/gmdd-8-791-2015-supplement.

Acknowledgements. This work was founded by the University of L'Aquila (Italy) and Regione Abruzzo in the frame of "High Formation Project" (P.O.F.S.E 2007–2013), and the Italian Space Agency in the frame of the PRIMES (contract I/017/11/0) project. Paolo Tuccella is grateful to the National and Oceanic Administration (NOAA) of Boulder (CO, USA) for the hospitality, and to Ravan Ahmadov and Stuart McKeen for the precious and profitable discussions about the parameterization for secondary organic aerosol. We are grateful to the Euro-Mediterranean Center on Climate Change (CMCC) for having made available their supercomputer to perform the numerical simulations. The authors thank Hugo Denier van der Gon for providing the TNO emissions.

References

Aan de Brugh, J. M. J., Henzing, J. S., Schaap, M., Morgan, W. T., van Heerwaarden, C. C., Weijers, E. P., Coe, H., and Krol, M. C.: Modelling the partitioning of ammonium nitrate in the convective boundary layer, Atmos. Chem. Phys., 12, 3005–3023, doi:10.5194/acp-12-3005-2012, 2012.

Abdul-Razzak, H. and Ghan, S. J.: A parameterization of aerosol activation: 2. Multiple aerosol types, J. Geophys. Res., 105, 6837–6844, doi:10.1029/1999JD901161, 2000.

Abdul-Razzak, H. and Ghan, S. J.: A parameterization of aerosol activation: 3. Sectional representation, J. Geophys. Res., 107, 4026, doi:10.1029/2001JD000483, 2002.

GMDD
8, 791–853, 2015

Ackermann, I. J., Hass, H., Memmsheimer, M., Ebel, A., Binkowski, F. S., and Shankar, U.: Modal aerosol dynamics model for Europe: development and first applications, Atmos. Environ., 32, 2981–2999, doi:10.1016/S1352-2310(98)00006-5, 1998.

Ahmadov, R., McKeen, S. A., Robinson, A., Bahreini, R., Middlebrook, A., de Gouw, J., Meagher, J., Hsie, E., Edgerton, E., Shaw, S., and Trainer, M.: A volatility basis set model for summertime secondary organic aerosols over the eastern United States in 2006, J. Geophys. Res., 117, D06301, doi:10.1029/2011JD016831, 2012.

Andreae, M. O, and Rosenfeld, D.: Aerosol–cloud–precipitation interactions. Part 1. The nature and sources of cloud-active aerosols, Earth-Sci. Rev., 89, 13–41, doi:10.1016/j.earscirev.2008.03.001, 2008.

Athanasopoulou, E., Vogel, H., Vogel, B., Tsimpidi, A. P., Pandis, S. N., Knote, C., and Fountoukis, C.: Modeling the meteorological and chemical effects of secondary organic aerosols during an EUCAARI campaign, Atmos. Chem. Phys., 13, 625–645, doi:10.5194/acp-13-625-2013, 2013.

Baklanov, A., Schlünzen, K., Suppan, P., Baldasano, J., Brunner, D., Aksoyoglu, S., Carmichael, G., Douros, J., Flemming, J., Forkel, R., Galmarini, S., Gauss, M., Grell, G., Hirtl, M., Joffre, S., Jorba, O., Kaas, E., Kaasik, M., Kallos, G., Kong, X., Korsholm, U., Kurganskiy, A., Kushta, J., Lohmann, U., Mahura, A., Manders-Groot, A., Maurizi, A., Moussiopoulos, N., Rao, S. T., Savage, N., Seigneur, C., Sokhi, R. S., Solazzo, E., Solomos, S., Sørensen, B., Tsegas, G., Vignati, E., Vogel, B., and Zhang, Y.: Online coupled regional meteorology chemistry models in Europe: current status and prospects, Atmos. Chem. Phys., 14, 317–398, doi:10.5194/acp-14-317-2014, 2014.

Balzarini, A., Pirovano, G., Honzak, L., Zabkar, R., Curci, G., Forkel, R., Hirtl, M., San José, R., Tuccella, P., and Grell, G. A.: WRF-Chem model sensitivity to chemical mechanism choice in reconstructing aerosol optical properties, Atmos. Environ., doi:10.1016/j.atmosenv.2014.12.033, in press, 2014.

Barnard, J. C., Fast, J. D., Paredes-Miranda, G., Arnott, W. P., and Laskin, A.: Technical Note: Evaluation of the WRF-Chem "Aerosol Chemical to Aerosol Optical Properties" Module using data from the MILAGRO campaign, Atmos. Chem. Phys., 10, 7325–7340, doi:10.5194/acp-10-7325-2010, 2010.

Bao, J.-W., Michelson, S. A., McKeen, S. A., and Grell, G. A.: Meteorological evaluation of a weather–chemistry forecasting model using observations from the TEXAS AQS 2000 field experiment, J. Geophys. Res., 110, D21105, doi:10.1029/2004JD005024, 2005.

GMDD
8, 791–853, 2015

Bègue, N., Tulet, P., Pelon, J., Aouizerats, B., Berger, A., and Schwarzenboeck, A.: Aerosol processing and CCN formation of an intense Saharan dust plume during the EUCAARI 2008 campaign, Atmos. Chem. Phys. Discuss., 14, 27039–27091, doi:10.5194/acpd-14-27039-2014, 2014.

Bei, N., Li, G., and Molina, L. T.: Uncertainties in SOA simulations due to meteorological uncertainties in Mexico City during MILAGRO-2006 field campaign, Atmos. Chem. Phys., 12, 11295–11308, doi:10.5194/acp-12-11295-2012, 2012.

Bessagnet, B., Seigneur, C., and Menut, L.: Impact of dry deposition of semi-volatile organic compounds on secondary organic aerosols, Atmos. Environ., 44, 1781–1787, doi:10.1016/j.atmosenv.2010.01.027, 2010.

Boucher, O., Randall, D., Artaxo, P., Bretherton, C., Feingold, G., Forster, P., Kerminen, V.-M., Kondo, Y., Liao, H., Lohmann, U., Rasch, P., Satheesh, S. K., Sherwood, S., Stevens, B., and Zhang, X. Y.: Clouds and aerosols, in: Climate Change 2013: the Physical Science Basis. Contribution of Working Group I to the Fifth Assessment Report of the Intergovernmental Panel on Climate Change, edited by: Stocker, T. F., Qin, D., Plattner, G.-K., Tignor, M., Allen, S. K., Boschung, J., Nauels, A., Xia, Y., Bex, V., and Midgley, P. M., Cambridge University Press, Cambridge, UK and New York, NY, USA, 2013.

Brunner, D., Jorba, O., Savage, N., Eder, B., Makar, P., Giordano, L., Badia, A., Balzarini, A., Baro, R., Bianconi, R., Chemel, C., Forkel, R., Jimenez-Guerrero, P., Hirtl, M., Hodzic, A., Honzak, L., Im, U., Knote, C., Kuenen, J. P. P., Makar, P. A., Manders-Groot, A., Neal, L., Perez, J. L., Pirovano, G., San Jose, R., Savage, N., Schroder, W., Sokhi, R. S., Syrakov, D., Torian, A., Tuccella, P., Werhahn, K., Wolke, R., van Meijgaard, E., Yahya, K., Zabkar, R., Zhang, Y., Zhang, J., Hogrefe, C., and Galmarini, S.: Evaluation of the meteorological performance of coupled chemistry–meteorology models in phase 2 of the air quality model evaluation international initiative, Atmos. Environ., doi:10.1016/j.atmosenv.2014.12.032, in press, 2014.

Christensen, M. W. and Stephens, G. L.: Microphysical and macrophysical responses of marine stratocumulus polluted by underlying ships: evidence of cloud deepening, J. Geophys. Res., 116, D03201, doi:10.1029/2010JD014638, 2011.

Clarke, A. and Kapustin, A.: Hemispheric aerosol vertical profiles: anthropogenic impacts on optical depth and cloud nuclei, Science, 329, 1488, doi:10.1126/science.1188838, 2010.

Crumeyrolle, S., Schwarzenboeck, A., Roger, J. C., Sellegri, K., Burkhart, J. F., Stohl, A., Gomes, L., Quennehen, B., Roberts, G., Weigel, R., Villani, P., Pichon, J. M., Bourri-

GMDD
8, 791–853, 2015

anne, T., and Laj, P.: Overview of aerosol properties associated with air masses sampled by the ATR-42 during the EUCAARI campaign (2008), Atmos. Chem. Phys., 13, 4877–4893, doi:10.5194/acp-13-4877-2013, 2013.

Curci, G., Ferrero, L., Tuccella, P., Barnaba, F., Angelini, F., Bolzacchini, E., Carbone, C., Denier van der Gon, H. A. C., Facchini, M. C., Gobbi, G. P., Kuenen, J. P. P., Landi, T. C., Perrino, C., Perrone, M. G., Sangiorgi, G., and Stocchi, P.: How much is particulate matter near the ground influenced by upper level processes within and above the PBL? A summertime case study in Milan (Italy), Atmos. Chem. Phys. Discuss., 14, 26403–26461, doi:10.5194/acpd-14-26403-2014, 2014a.

Curci, G., Hogrefe, C., Bianconi, R., Im, U., Balzarini, A., Baro, R., Brunner, D., Forkel, R., Giordano, L., Hirtl, M., Honzak, L., Jimenez-Guerrero, P., Knote, C., Langer, M., Makar, P. A., Pirovano, G., Perez, J. L., San Jose, R., Syrakov, D., Tuccella, P., Werhahn, J., Wolke, R., Zabkar, R., Zhang, J., Galmarini, S.: Uncertainties of simulated aerosol optical properties induced by assumptions on aerosol physical and chemical properties: an AQMEII-2 perspective, Atmos. Environ., doi:10.1016/j.atmosenv.2014.09.009, in press, 2014b.

Easter, R. C., Ghan, S. J., Zhang, Y., Saylor, R. D., Chapman, E. G., Laulainen, N. S., Abdul-Razzak, H., Leung, L. R., Bian, X., and Zaveri, R. A.: MIRAGE: model description and evaluation of aerosols and trace gases, J. Geophys. Res., 109, D20210, doi:10.1029/2004JD004571, 2004.

Ebert, E. E. and Curry, J. A.: A parameterization of ice cloud optical properties for climate models, J. Geophys. Res., 97, 3831–3836, doi:10.1029/91JD02472, 1992.

Elleman, R. A. and Covert, D. S.: Aerosol size distribution modeling with the Community Multiscale Air Quality modeling system in the Pacific Northwest: 3. Size distribution of particles emitted into a mesoscale model, J. Geophys. Res., 115, D03204, doi:10.1029/2009JD012401, 2010.

Emmons, L. K., Walters, S., Hess, P. G., Lamarque, J.-F., Pfister, G. G., Fillmore, D., Granier, C., Guenther, A., Kinnison, D., Laepple, T., Orlando, J., Tie, X., Tyndall, G., Wiedinmyer, C., Baughcum, S. L., and Kloster, S.: Description and evaluation of the Model for Ozone and Related chemical Tracers, version 4 (MOZART-4), Geosci. Model Dev., 3, 43–67, doi:10.5194/gmd-3-43-2010, 2010.

Ervens, B., Turpin, B. J., and Weber, R. J.: Secondary organic aerosol formation in cloud droplets and aqueous particles (aqSOA): a review of laboratory, field and model studies, Atmos. Chem. Phys., 11, 11069–11102, doi:10.5194/acp-11-11069-2011, 2011.

GMDD
8, 791–853, 2015

Fast, J. D., Allan, J., Bahreini, R., Craven, J., Emmons, L., Ferrare, R., Hayes, P. L., Hodzic, A., Holloway, J., Hostetler, C., Jimenez, J. L., Jonsson, H., Liu, S., Liu, Y., Metcalf, A., Middlebrook, A., Nowak, J., Pekour, M., Perring, A., Russell, L., Sedlacek, A., Seinfeld, J., Setyan, A., Shilling, J., Shrivastava, M., Springston, S., Song, C., Subramanian, R., Taylor, J. W., Vinoj, V., Yang, Q., Zaveri, R. A., and Zhang, Q.: Modeling regional aerosol and aerosol precursor variability over California and its sensitivity to emissions and long-range transport during the 2010 CalNex and CARES campaigns, Atmos. Chem. Phys., 14, 10013–10060, doi:10.5194/acp-14-10013-2014, 2014.

Fountoukis, C., Megaritis, A. G., Skyllakou, K., Charalampidis, P. E., Pilinis, C., Denier van der Gon, H. A. C., Crippa, M., Canonaco, F., Mohr, C., Prévôt, A. S. H., Allan, J. D., Poulain, L., Petäjä, T., Tiitta, P., Carbone, S., Kiendler-Scharr, A., Nemitz, E., O'Dowd, C., Swietlicki, E., and Pandis, S. N.: Organic aerosol concentration and composition over Europe: insights from comparison of regional model predictions with aerosol mass spectrometer factor analysis, Atmos. Chem. Phys., 14, 9061–9076, doi:10.5194/acp-14-9061-2014, 2014.

Ghan, S. J., Leung, L. R., Easter, R. C., and Abdul-Razzak, H.: Prediction of droplet number in a general circulation model, J. Geophys. Res., 102, 21777–21794, doi:10.1029/97JD01810, 1997.

Grell, G. A., Peckham, S. E., McKeen, S., Schmitz, R., Frost, G., Skamarock, W. C., and Eder, B.: Fully coupled "online" chemistry within the WRF model, Atmos. Environ., 39, 6957–6975, doi:10.1016/j.atmosenv.2005.04.027, 2005.

Guenther, A., Karl, T., Harley, P., Wiedinmyer, C., Palmer, P. I., and Geron, C.: Estimates of global terrestrial isoprene emissions using MEGAN (Model of Emissions of Gases and Aerosols from Nature), Atmos. Chem. Phys., 6, 3181–3210, doi:10.5194/acp-6-3181-2006, 2006.

Luo, G. and Yu, F.: Simulation of particle formation and number concentration over the Eastern United States with the WRF-Chem + APM model, Atmos. Chem. Phys., 11, 11521–11533, doi:10.5194/acp-11-11521-2011, 2011.

Hallquist, M., Wenger, J. C., Baltensperger, U., Rudich, Y., Simpson, D., Claeys, M., Dommen, J., Donahue, N. M., George, C., Goldstein, A. H., Hamilton, J. F., Herrmann, H., Hoffmann, T., Iinuma, Y., Jang, M., Jenkin, M. E., Jimenez, J. L., Kiendler-Scharr, A., Maenhaut, W., McFiggans, G., Mentel, Th. F., Monod, A., Prévôt, A. S. H., Seinfeld, J. H., Surratt, J. D., Szmigielski, R., and Wildt, J.: The formation, properties and impact of sec-

GMDD
8, 791–853, 2015

ondary organic aerosol: current and emerging issues, Atmos. Chem. Phys., 9, 5155–5236, doi:10.5194/acp-9-5155-2009, 2009.
Haywood, J. and Boucher, O.: Estimates of the direct and indirect aerosol radiative forcing due to tropospheric aerosols: a review, Rev. Geophys., 38, 513–543, doi:10.1029/1999RG000078, 2000.
Hamburger, T., McMeeking, G., Minikin, A., Birmili, W., Dall'Osto, M., O'Dowd, C., Flentje, H., Henzing, B., Junninen, H., Kristensson, A., de Leeuw, G., Stohl, A., Burkhart, J. F., Coe, H., Krejci, R., and Petzold, A.: Overview of the synoptic and pollution situation over Europe during the EUCAARI-LONGREX field campaign, Atmos. Chem. Phys., 11, 1065–1082, doi:10.5194/acp-11-1065-2011, 2011.
Hansen, J., Sato, M., and Ruedy, R.: Radiative forcing and climate response, J. Geophys. Res., 102, 6831–6894, doi:10.1029/96JD03436,1997.
Henrich, F., Siebert, H., Jakel, E., Shaw, R. A., and Wendisch, M.: Collocated measurements of boundary layer cloud microphysical and radiative properties: a feasibility study, J. Geophys. Res., 115, D24214, doi:10.1029/2010JD013930, 2010.
Holt, T. R., Niyogi, D., Chen, F., Manning, K., LeMone, M. A., and Qureshi, A.: Effect of land–atmosphere interactions on the IHOP 24–25 May 2002 convection case, Mon. Weather Rev., 134, 113–133, doi:10.1175/MWR3057.1, 2006.
King, N. J., Bower, K. N., Crosier, J., and Crawford, I.: Evaluating MODIS cloud retrievals with in situ observations from VOCALS-REx, Atmos. Chem. Phys., 13, 191–209, doi:10.5194/acp-13-191-2013, 2013.
Knote, C., Brunner, D., Vogel, H., Allan, J., Asmi, A., Äijälä, M., Carbone, S., van der Gon, H. D., Jimenez, J. L., Kiendler-Scharr, A., Mohr, C., Poulain, L., Prévôt, A. S. H., Swietlicki, E., and Vogel, B.: Towards an online-coupled chemistry-climate model: evaluation of trace gases and aerosols in COSMO-ART, Geosci. Model Dev., 4, 1077–1102, doi:10.5194/gmd-4-1077-2011, 2011.
Knote, C., Tuccella, P., Curci, G., Emmons, L., Orlando, J. J., Madronich, S., Barò, R., Jimìenez-Guerrero, P., Luecken, D., Hogrefe, C., Forkel, R., Werhahn, J., Hirtl, M., Pìrez, J. L., San Josée, R., Giordano, L., Brunner, D., Yahya, K., and Zhang, Y.: Influence of the choice of gas-phase mechanism on predictions of key gaseous pollutants during the AQMEII phase-2 intercomparison, Atmos. Environ., doi:doi:10.1016/j.atmosenv.2014.11.066, in press, 2014.

GMDD
8, 791–853, 2015

Knote, C., Hodzic, A., and Jimenez, J. L.: The effect of dry and wet deposition of condensable vapors on secondary organic aerosols concentrations over the continental US, Atmos. Chem. Phys., 15, 1–18, doi:10.5194/acp-15-1-2015, 2015.

Koren, I., Altaratz, O., Remer, L. A., Feingold, G., Martins, J. V., and Heiblum, R. H.: Aerosol-induced intensification of rain from the tropics to the mid-latitudes, Nat. Geosci., 5, 118–122, doi:10.1038/ngeo1364, 2012.

Kuenen, J. J. P., Visschedijk, A. J. H., Jozwicka, M., and Denier van der Gon, H. A. C.: TNO-MACC_II emission inventory; a multi-year (2003–2009) consistent high-resolution European emission inventory for air quality modelling, Atmos. Chem. Phys., 14, 10963–10976, doi:10.5194/acp-14-10963-2014, 2014.

Kulmala, M., Asmi, A., Lappalainen, H. K., Baltensperger, U., Brenguier, J.-L., Facchini, M. C., Hansson, H.-C., Hov, Ø., O'Dowd, C. D., Pöschl, U., Wiedensohler, A., Boers, R., Boucher, O., de Leeuw, G., Denier van der Gon, H. A. C., Feichter, J., Krejci, R., Laj, P., Lihavainen, H., Lohmann, U., McFiggans, G., Mentel, T., Pilinis, C., Riipinen, I., Schulz, M., Stohl, A., Swietlicki, E., Vignati, E., Alves, C., Amann, M., Ammann, M., Arabas, S., Artaxo, P., Baars, H., Beddows, D. C. S., Bergström, R., Beukes, J. P., Bilde, M., Burkhart, J. F., Canonaco, F., Clegg, S. L., Coe, H., Crumeyrolle, S., D'Anna, B., Decesari, S., Gilardoni, S., Fischer, M., Fjaeraa, A. M., Fountoukis, C., George, C., Gomes, L., Halloran, P., Hamburger, T., Harrison, R. M., Herrmann, H., Hoffmann, T., Hoose, C., Hu, M., Hyvärinen, A., Hõrrak, U., Iinuma, Y., Iversen, T., Josipovic, M., Kanakidou, M., Kiendler-Scharr, A., Kirkevåg, A., Kiss, G., Klimont, Z., Kolmonen, P., Komppula, M., Kristjánsson, J.-E., Laakso, L., Laaksonen, A., Labonnote, L., Lanz, V. A., Lehtinen, K. E. J., Rizzo, L. V., Makkonen, R., Manninen, H. E., McMeeking, G., Merikanto, J., Minikin, A., Mirme, S., Morgan, W. T., Nemitz, E., O'Donnell, D., Panwar, T. S., Pawlowska, H., Petzold, A., Pienaar, J. J., Pio, C., Plass-Duelmer, C., Prévôt, A. S. H., Pryor, S., Reddington, C. L., Roberts, G., Rosenfeld, D., Schwarz, J., Seland, Ø., Sellegri, K., Shen, X. J., Shiraiwa, M., Siebert, H., Sierau, B., Simpson, D., Sun, J. Y., Topping, D., Tunved, P., Vaattovaara, P., Vakkari, V., Veefkind, J. P., Visschedijk, A., Vuollekoski, H., Vuolo, R., Wehner, B., Wildt, J., Woodward, S., Worsnop, D. R., van Zadelhoff, G.-J., Zardini, A. A., Zhang, K., van Zyl, P. G., Kerminen, V.-M., S Carslaw, K., and Pandis, S. N.: General overview: European Integrated project on Aerosol Cloud Climate and Air Quality interactions (EUCAARI) – integrating aerosol research from nano to global scales, Atmos. Chem. Phys., 11, 13061–13143, doi:10.5194/acp-11-13061-2011, 2011.

GMDD
8, 791–853, 2015

Lecœur, È. and Seigneur, C.: Dynamic evaluation of a multi-year model simulation of particulate matter concentrations over Europe, Atmos. Chem. Phys., 13, 4319–4337, doi:10.5194/acp-13-4319-2013, 2013.

Lee, L. A., Pringle, K. J., Reddington, C. L., Mann, G. W., Stier, P., Spracklen, D. V., Pierce, J. R., and Carslaw, K. S.: The magnitude and causes of uncertainty in global model simulations of cloud condensation nuclei, Atmos. Chem. Phys., 13, 8879–8914, doi:10.5194/acp-13-8879-2013, 2013.

Li, X., Rohrer, F., Hofzumahaus, A., Brauers, T., Häseler, R., Bohn, B., Broch, S., Fuchs, H., Gomm, S., Holland, F., Jäger, J., Kaiser, J., Keutsch, F. N., Lohse, I., Lu, K., Tillmann, R., Wegener, R., Wolfe, G. M., Mentel, F. M., Kiendler-Scharr, A., and Wahner, A.: Missing gas-phase source of HONO inferred from zeppelin measurements in the troposphere, Science, 344, 292–296, doi:10.1126/science.1248999, 2014.

Li, Y. P., Elbern, H., Lu, K. D., Friese, E., Kiendler-Scharr, A., Mentel, Th. F., Wang, X. S., Wahner, A., and Zhang, Y. H.: Updated aerosol module and its application to simulate secondary organic aerosols during IMPACT campaign May 2008, Atmos. Chem. Phys., 13, 6289–6304, doi:10.5194/acp-13-6289-2013, 2013.

Li, Z., Niu, F., Fan, J., Liu, Y., Rosenfeld, D., and Ding, D.: Long-term impacts of aerosols on the vertical development of clouds and precipitation, Nat. Geosci., 4, 888–894, doi:10.1038/ngeo1313, 2011.

Lohmann, U. and Feichter, J.: Global indirect aerosol effects: a review, Atmos. Chem. Phys., 5, 715–737, doi:10.5194/acp-5-715-2005, 2005.

McKeen, S., Chung, S. H., Wilczak, J., Grell, G., Djalalova, I., Peckham, S., Gong, W., Bouchet, V., Moffet, R., Tang, Y., Carmichael, G. R., Mathur, R., and Yu, S.: Evaluation of several $PM_{2.5}$ forecast models using data collected during the ICARTT/NEAQS 2004 field study, J. Geophys. Res., 112, D10S20, doi:10.1029/2006JD007608, 2007.

Meng, Z., Dabdud, D., and Seinfeld, J. H.: Chemical coupling between atmospheric ozone and particulate matter, Science, 277, 116–119, doi:10.1126/science.277.5322.116, 1997.

Mensah, A. A., Holzinger, R., Otjes, R., Trimborn, A., Mentel, Th. F., ten Brink, H., Henzing, B., and Kiendler-Scharr, A.: Aerosol chemical composition at Cabauw, The Netherlands as observed in two intensive periods in May 2008 and March 2009, Atmos. Chem. Phys., 12, 4723–4742, doi:10.5194/acp-12-4723-2012, 2012.

GMDD
8, 791–853, 2015

Merikanto, J., Spracklen, D. V., Mann, G. W., Pickering, S. J., and Carslaw, K. S.: Impact of nucleation on global CCN, Atmos. Chem. Phys., 9, 8601–8616, doi:10.5194/acp-9-8601-2009, 2009.

Misenis, C. and Zhang, Y.: An examination of sensitivity of WRF/Chem predictions to physical parameterizations, horizontal grid spacing, and nesting options, Atmos. Res., 97, 315–334, doi:10.1016/j.atmosres.2010.04.005, 2010.

Ngan, F., Kim, H., Lee, P., Al-Wali, K., and Dornblaser, B.: A study of nocturnal surface wind speed overprediction by the WRF-ARW model in southeastern Texas, J. Appl. Meteorol. Clim., 52, 2638–2653, doi:10.1175/JAMC-D-13-060.1, 2013.

O'Donnell, D., Tsigaridis, K., and Feichter, J.: Estimating the direct and indirect effects of secondary organic aerosols using ECHAM5-HAM, Atmos. Chem. Phys., 11, 8635–8659, doi:10.5194/acp-11-8635-2011, 2011.

Otkin, J. A. and Greenwald, T. J.: Comparison of WRF model-simulated and MODIS-derived cloud data, Mon. Weather Rev., 136, 1957–1970, doi:10.1175/2007MWR2293.1, 2008.

Painemal, D. and Zuidema, P.: Assessment of MODIS cloud effective radius and optical thickness retrievals over the Southeast Pacific with VOCALS-REx in situ measurements, J. Geophys. Res., 116, D24206, doi:10.1029/2011JD016155, 2011.

Pielke, R. A.: Influence of the spatial distribution of vegetation and soils on the prediction of cumulus convective rainfall, Rev. Geophys., 39, doi:10.1029/1999RG000072, 2001.

Pierce, J. R. and Adams, P. J.: Uncertainty in global CCN concentrations from uncertain aerosol nucleation and primary emission rates, Atmos. Chem. Phys., 9, 1339–1356, doi:10.5194/acp-9-1339-2009, 2009.

Roelofs, G.-J., ten Brink, H., Kiendler-Scharr, A., de Leeuw, G., Mensah, A., Minikin, A., and Otjes, R.: Evaluation of simulated aerosol properties with the aerosol-climate model ECHAM5-HAM using observations from the IMPACT field campaign, Atmos. Chem. Phys., 10, 7709–7722, doi:10.5194/acp-10-7709-2010, 2010.

Rosenfeld, D., Lohmann, U., Raga, G. B., O'Dowd, C. D., Kulmala, M., Fuzzi, S., Reissel, A., and Andreae, M. O.: Flood or drought: how do aerosols affect precipitation?, Science, 321, 1308–1313, doi:10.1126/science.1160606, 2008.

Saide, P. E., Spak, S. N., Carmichael, G. R., Mena-Carrasco, M. A., Yang, Q., Howell, S., Leon, D. C., Snider, J. R., Bandy, A. R., Collett, J. L., Benedict, K. B., de Szoeke, S. P., Hawkins, L. N., Allen, G., Crawford, I., Crosier, J., and Springston, S. R.: Evaluating WRF-

GMDD
8, 791–853, 2015

Chem aerosol indirect effects in Southeast Pacific marine stratocumulus during VOCALS-REx, Atmos. Chem. Phys., 12, 3045–3064, doi:10.5194/acp-12-3045-2012, 2012.
Schell, B., Ackermann, I. J., Hass, H., Binkowski, F. S., and Ebel, A.: Modeling the formation of secondary organic aerosol within a comprehensive air quality model system, J. Geophys. Res., 106, 28275–28293, doi:10.1029/2001JD000384, 2001.
Scott, C. E., Rap, A., Spracklen, D. V., Forster, P. M., Carslaw, K. S., Mann, G. W., Pringle, K. J., Kivekäs, N., Kulmala, M., Lihavainen, H., and Tunved, P.: The direct and indirect radiative effects of biogenic secondary organic aerosol, Atmos. Chem. Phys., 14, 447–470, doi:10.5194/acp-14-447-2014, 2014.
Sotiropoulou, R. E. P., Tagaris, E., Pilinis, C., Anttila, T., and Kulmala, M.: Modeling new particle formation during air pollution episodes: Impacts on aerosol and cloud condensation nuclei, Aerosol Sci. Tech., 40, 557–572, doi:10.1080/02786820600714346, 2006.
Spracklen, D. V., Carslaw, K. S., Kulmala, M., Kerminen, V.-M., Mann, G. W., and Sihto, S.-L.: The contribution of boundary layer nucleation events to total particle concentrations on regional and global scales, Atmos. Chem. Phys., 6, 5631–5648, doi:10.5194/acp-6-5631-2006, 2006.
Stern, R., Builtjes, P., Shaap, M., Timmermans, R., Vautard, R., Hodzic, A., Memmesheimer, M., Feldmann, H., Renner, E., Wolke, R., and Kershbaumer, A.: A model inter-comparison study focussing on episode with elevated PM_{10} concentrations, Atmos. Environ., 42, 4567–4588, doi:10.1016/j.atmosenv.2008.01.068, 2008.
Stockwell, W. R., Middleton, P., Chang, J. S., and Tang, X.: The second-generation regional acid deposition model chemical mechanism for regional air quality modeling, J. Geophys. Res., 95, 16343–16367, doi:10.1029/JD095iD10p16343, 1990.
Ten Hoeve, J. E., Remer, L. A., and Jacobson, M. Z.: Microphysical and radiative effects of aerosols on warm clouds during the Amazon biomass burning season as observed by MODIS: impacts of water vapor and land cover, Atmos. Chem. Phys., 11, 3021–3036, doi:10.5194/acp-11-3021-2011, 2011.
Tuccella, P., Curci, G., Visconti, G., Bessagnet, B., Menut, L., and Park, R. J.: Modeling of gas and aerosol with WRF/Chem over Europe: evaluation and sensitivity study, J. Geophys. Res., 117, D03303, doi:10.1029/2011JD016302, 2012.
Turpin, B. J. and Lim, H.-J.: Species contributions to $PM_{2.5}$ mass concentrations: revisiting common assumptions for estimating organic mass, Aerosol Sci. Tech., 35, 602–610, doi:10.1080/02786820152051454, 2001.

GMDD
8, 791–853, 2015

Walcek, C. J. and Taylor, G. R.: A theoretical method for computing vertical distributions of acidity and sulfate production within cumulus clouds, J. Atmos Sci., 43, 339–355, doi:10.1175/1520-0469(1986)043$<$0339:ATMFCV$>$2.0.CO;2, 1986.

Yang, Q., W. I. Gustafson Jr., Fast, J. D., Wang, H., Easter, R. C., Morrison, H., Lee, Y.-N., Chapman, E. G., Spak, S. N., and Mena-Carrasco, M. A.: Assessing regional scale predictions of aerosols, marine stratocumulus, and their interactions during VOCALS-REx using WRF-Chem, Atmos. Chem. Phys., 11, 11951–11975, doi:10.5194/acp-11-11951-2011, 2011.

Yu, S., Mathur, R., Pleim, J., Wong, D., Gilliam, R., Alapaty, K., Zhao, C., and Liu, X.: Aerosol indirect effect on the grid-scale clouds in the two-way coupled WRF–CMAQ: model description, development, evaluation and regional analysis, Atmos. Chem. Phys., 14, 11247–11285, doi:10.5194/acp-14-11247-2014, 2014.

Zhang, Y.: Online-coupled meteorology and chemistry models: history, current status, and outlook, Atmos. Chem. Phys., 8, 2895–2932, doi:10.5194/acp-8-2895-2008, 2008.

Zhang, Y., Sartelet, K., Wu, S.-Y., and Seigneur, C.: Application of WRF/Chem-MADRID and WRF/Polyphemus in Europe – Part 1: Model description, evaluation of meteorological predictions, and aerosol–meteorology interactions, Atmos. Chem. Phys., 13, 6807–6843, doi:10.5194/acp-13-6807-2013, 2013a.

Zhang, Y., Sartelet, K., Zhu, S., Wang, W., Wu, S.-Y., Zhang, X., Wang, K., Tran, P., Seigneur, C., and Wang, Z.-F.: Application of WRF/Chem-MADRID and WRF/Polyphemus in Europe – Part 2: Evaluation of chemical concentrations and sensitivity simulations, Atmos. Chem. Phys., 13, 6845–6875, doi:10.5194/acp-13-6845-2013, 2013b.

Zhao, C., Liu, X., Leung, L. R., Johnson, B., McFarlane, S. A., Gustafson Jr., W. I., Fast, J. D., and Easter, R.: The spatial distribution of mineral dust and its shortwave radiative forcing over North Africa: modeling sensitivities to dust emissions and aerosol size treatments, Atmos. Chem. Phys., 10, 8821–8838, doi:10.5194/acp-10-8821-2010, 2010.

GMDD
8, 791–853, 2015

Table 1. Physical and chemical parameterizations used in the simulation.

Physical Processes	WRF/Chem parameterizations
Cloud Microphysics	Morrison
Cumulus Cloud	New Grell (D1 and D2)
Longwave radiation	RRTM
Shortwave radiation	RRTM
PBL	MYNN
Surface Layer	Monin–Obukov
Surface	Noah LSM
Gas-phase Chemistry	Modified RACM-ESRL
Aerosol Chemistry	MADE/SOA-VBS
Biogenic Emissions	MEGAN

GMDD
8, 791–853, 2015

Table 2. Statistical indices of the comparison of WRF/Chem to meteorological and chemical observations collected at Cabauw tower.

Variable	r	MB	NMB	NMGE
T2 (°C)	0.93	−0.66	−5.46	10.65
T10 (°C)	0.93	−0.67	−5.24	9.31
T20 (°C)	0.94	−0.56	−4.15	8.16
T40 (°C)	0.94	−0.46	−3.24	7.21
T80 (°C)	0.95	−0.32	−2.10	5.97
T140 (°C)	0.95	−0.26	−1.51	5.92
T200 (°C)	0.95	−0.45	−2.79	6.66
RH2 (%)	0.87	3.17	6.42	11.23
RH10 (%)	0.89	4.44	8.36	11.48
RH2 (%)	0.91	3.04	6.33	10.50
RH40 (%)	0.92	2.99	6.40	10.51
RH80 (%)	0.73	−1.4	2.13	13.34
RH140 (%)	0.92	2.81	6.40	11.19
RH200 (%)	0.91	2.99	7.44	12.50
WS10 (ms^{-1})	0.78	0.67	27.90	35.56
WS20 (ms^{-1})	0.66	1.27	40.89	49.32
WS40 (ms^{-1})	0.67	1.26	32.64	42.04
WS80 (ms^{-1})	0.72	1.23	24.42	38.99
WS140 (ms^{-1})	0.74	1.21	28.66	41.55
WS200 (ms^{-1})	0.76	1.13	27.79	41.48
WD10 (deg)	0.52	27.32	43.31	43.31
WD20 (deg)	0.53	24.80	40.48	40.48
WD40 (deg)	0.60	23.59	4.34	40.34
WD80 (deg)	0.67	20.22	30.34	30.34
WD140 (deg)	0.71	19.21	32.01	32.01
WS200 (deg)	0.73	17.18	28.46	28.46
O_3 ($\mu g m^{-3}$)	0.72	−3.43	70.03	90.88
NO_x ($\mu g m^{-3}$)	0.70	0.43	19.76	44.77
NO ($\mu g m^{-3}$)	0.65	0.28	116.08	167.59
NO_2 ($\mu g m^{-3}$)	0.66	1.25	28.68	54.20
NH_3 ($\mu g m^{-3}$)	0.43	−4.75	−27.72	42.94
HNO_3 ($\mu g m^{-3}$)	0.21	−0.09	−1.22	108.65
HONO ($\mu g m^{-3}$)	0.05	−0.56	−95.37	95.37
SO_2 ($\mu g m^{-3}$)	0.48	0.68	90.20	116.33
SO_4 ($\mu g m^{-3}$)	0.56	1.04	92.2	95.4
NO_3 ($\mu g m^{-3}$)	0.68	1.00	72.4	94.3
NH_4 ($\mu g m^{-3}$)	0.74	0.66	63.	67.3
OM ($\mu g m^{-3}$)	0.75	−0.42	3.21	29.9

GMDD
8, 791–853, 2015

Table 3. Observed and modelled mean values, SDs, and relative amount (expressed as %) of aerosol species, number of aerosol particles, cloud condensation nuclei, over the whole period of the aircraft campaign in boundary layer and free troposphere.

	Boundary Layer			Free Troposphere		
	Observation	WRF/Chem	r	Observation	WRF/Chem	r
SO_4 ($\mu g\,m^{-3}$)	3.1 ± 2.4 (19 %)	3.2 ± 2.1 (24 %)	0.39	2.6 ± 2. (29 %)	2.5 ± 1.2 (38 %)	0.23
NO_3 ($\mu g\,m^{-3}$)	4.5 ± 5.4 (28 %)	4.6 ± 5.1 (34 %)	0.47	1.3 ± 3. (14 %)	1.5 ± 2.7 (23 %)	0.44
NH_4 ($\mu g\,m^{-3}$)	2.6 ± 2.2 (16 %)	2.4 ± 2.1 (19 %)	0.43	1.4 ± 1.5 (16 %)	1.2 ± 1.2 (19 %)	0.42
OM ($\mu g\,m^{-3}$)	6.1 ± 5.8 (37 %)	3.0 ± 2.6 (23 %)	0.67	3.7 ± 4.5 (41 %)	1.3 ± 1.4 (20 %)	0.52
CN (10^3 # cm^{-3})	6.7 ± 5.	9.4 ± 5.4	0.40	1. ± 1.1	1.7 ± 2.8	0.74
CCN (10^3 # cm^{-3})	0.6 ± 0.5	0.9 ± 0.8	0.45	0.3 ± 0.3	0.3 ± 0.3	0.73

GMDD
8, 791–853, 2015

Table 4. MODIS and modelled mean values and SDs of cloud water path and cloud optical thickness, on 17 and 25 May 2008.

	CWP ($g\,m^{-2}$)		COT	
	MODIS-Aqua	WRF/Chem	MODIS-Aqua	WRF/Chem
17 May 2008	340 ± 225	595 ± 775	37 ± 22	40 ± 38
25 May 2008	270 ± 225	475 ± 760	24 ± 19	22 ± 28

GMDD
8, 791–853, 2015

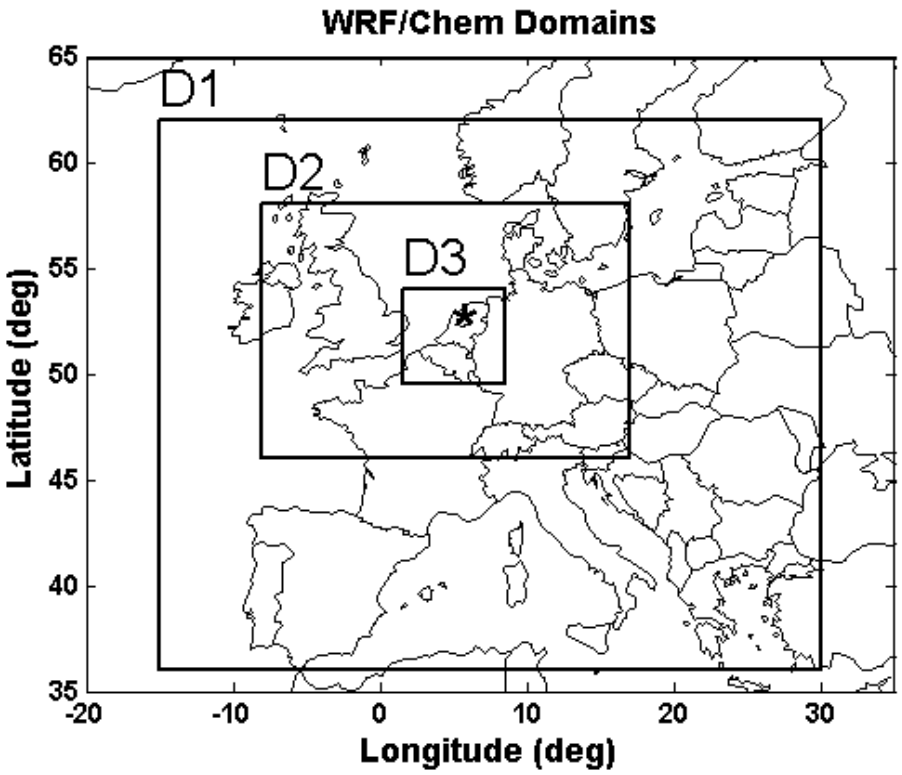

Figure 1. The three nested model domains used for simulations. D1 is 30 km resolution, D2 10 km, and D3 2 km. The black star indicates the Cabauw supersite.

GMDD
8, 791–853, 2015

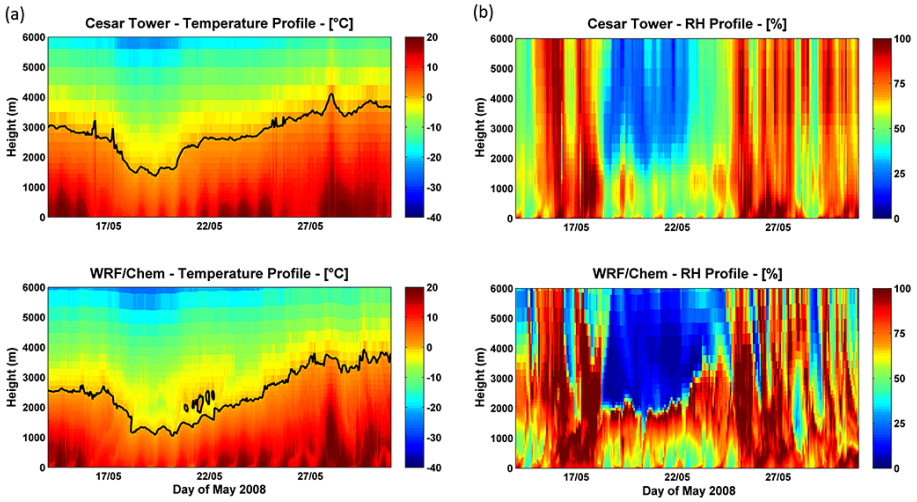

Figure 2. Observed and simulated time series of vertical profile of the temperature **(a)** and relative humidity **(b)**, observed at Cesar observatory. The black line on the temperature profile represents the 0 °C isotherm.

GMDD
8, 791–853, 2015

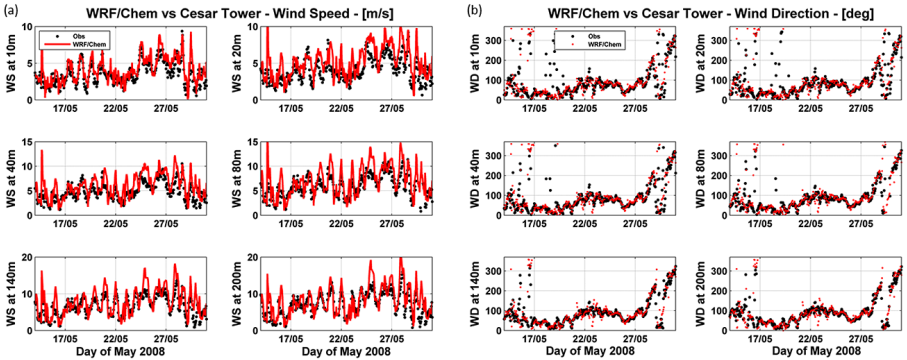

Figure 3. Observed (black lines) and simulated (red lines) time series of wind speed **(a)** and wind direction **(b)** at different height at Cesar Tower.

GMDD
8, 791–853, 2015

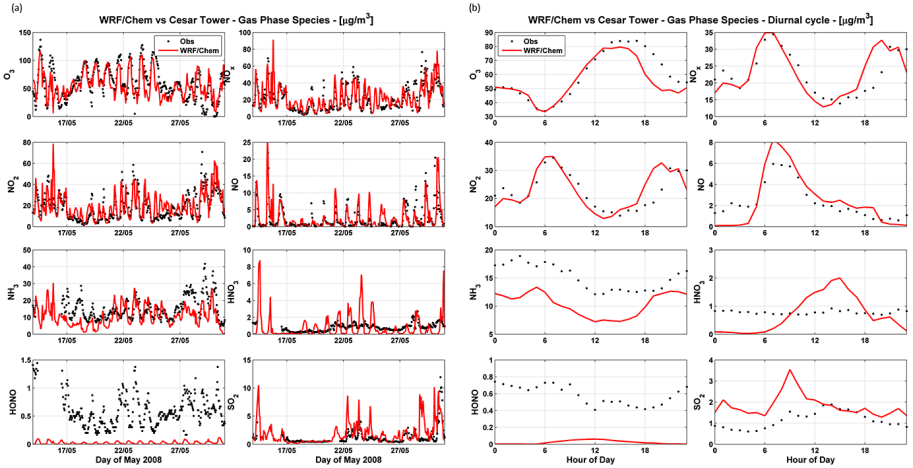

Figure 4. Observed and simulated time series of gas-phase species **(a)** and their average diurnal cycle **(b)**, at EMEP station (NL0011R).

GMDD
8, 791–853, 2015

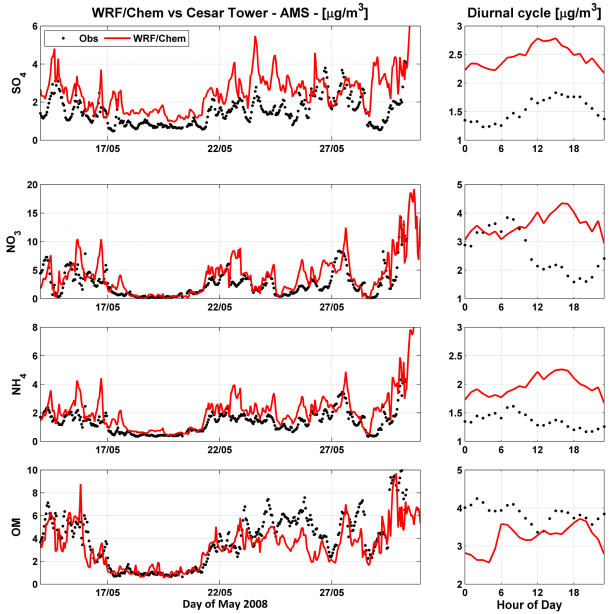

Figure 5. As Fig. 4, but for aerosol mass speciation at Cesar Observatory at 60 m of height.

GMDD
8, 791–853, 2015

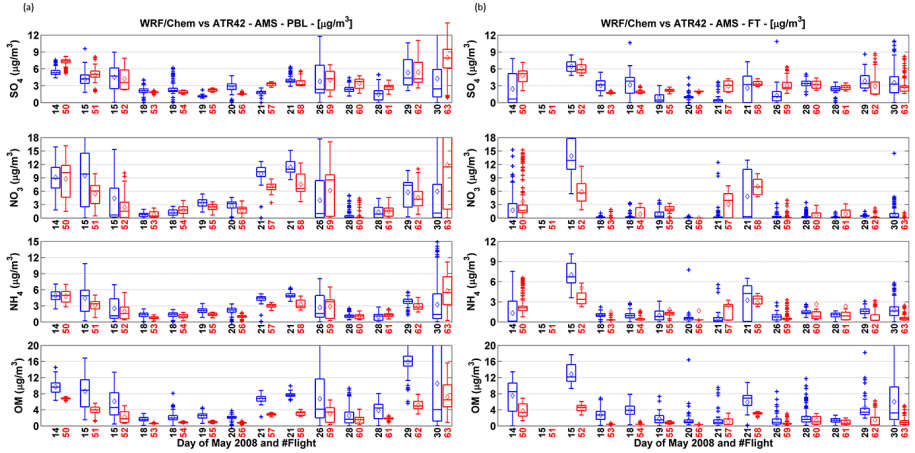

Figure 6. Box plot of SO_4, NO_3, NH_4, and OM mass concentrations measured by AMS aboard the ATR-42 (blue) and simulated by WRF/Chem (red) within boundary layer **(a)** and free troposphere **(b)**. The *x* axis reports the day of May 2008 (black) and the number of the research flight (red). The whisker plots denote median, 25th and 75th percentiles, 1.5× (inter-quartile range), and outliers. The squares represent the mean values.

GMDD
8, 791–853, 2015

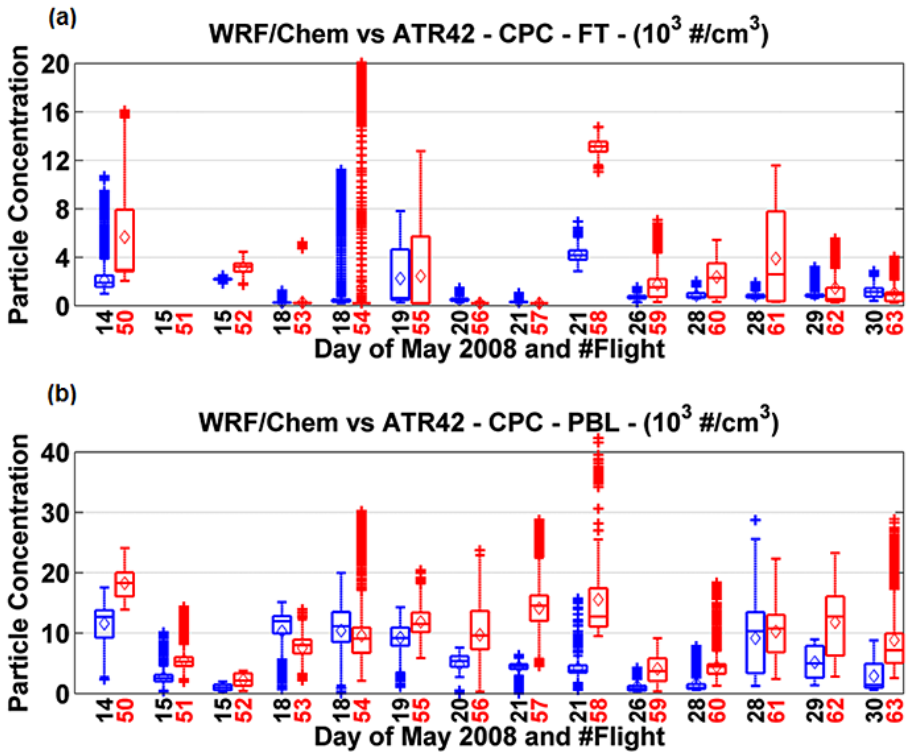

Figure 7. Same as Fig. 6 but for comparison of observed and simulated condensation nuclei (CN) concentration.

GMDD
8, 791–853, 2015

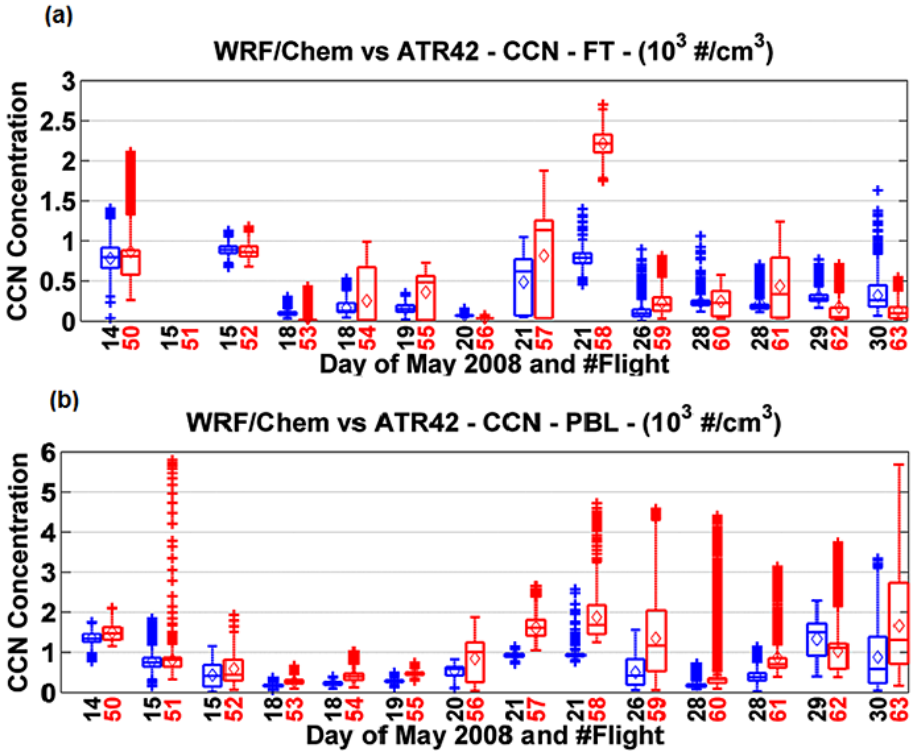

Figure 8. Same as Fig. 6 but for comparison of observed and simulated cloud condensation nuclei (CCN) concentration at 0.2 % of supersaturation.

GMDD
8, 791–853, 2015

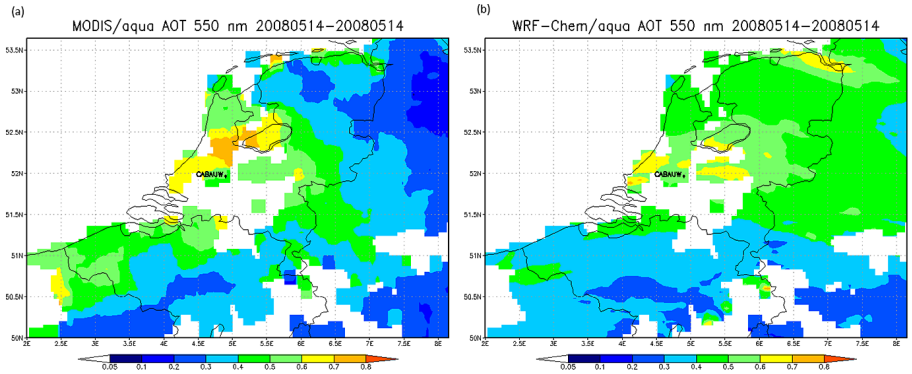

Figure 9. Aerosol optical thickness at 500 nm from MODIS-Aqua **(a)** and WRF/Chem simulations **(b)** on 14 May 2008.

GMDD
8, 791–853, 2015

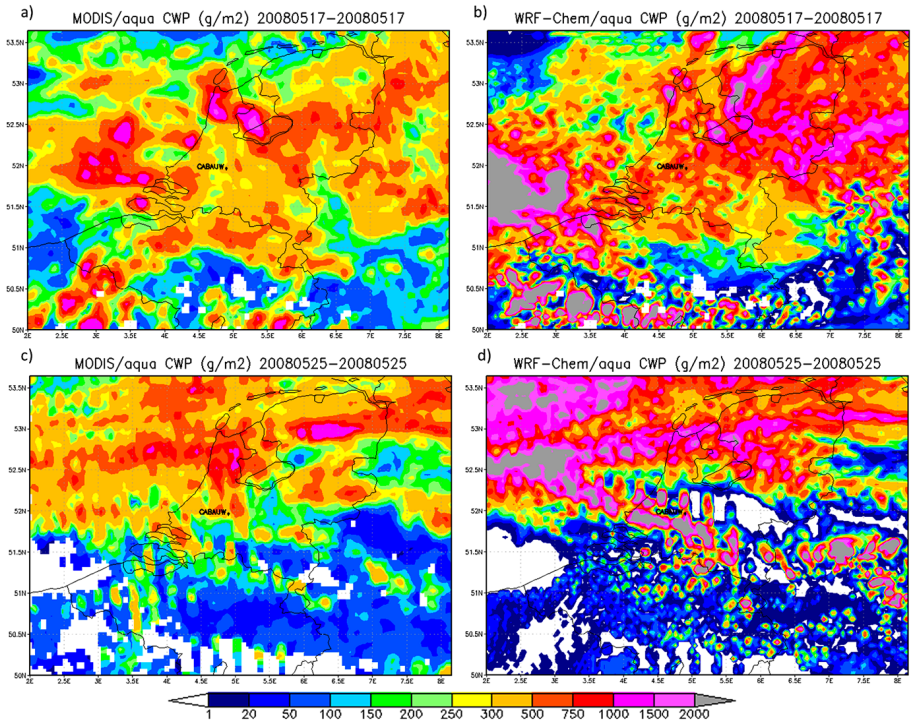

Figure 10. Cloud water path on 17 (first row) and 25 (second row) May 2008 from MODIS-Aqua (**a** and **c**) and WRF/Chem simulations (**b** and **d**).

GMDD
8, 791–853, 2015

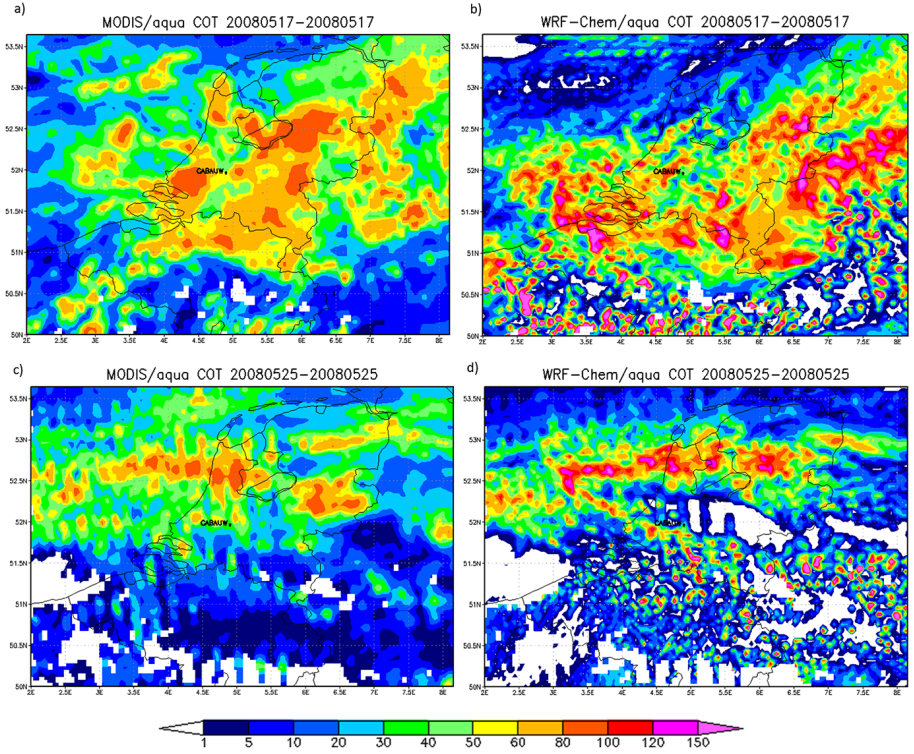

Figure 11. Same as Fig. 10 but for cloud optical thickness.

GMDD
8, 791–853, 2015

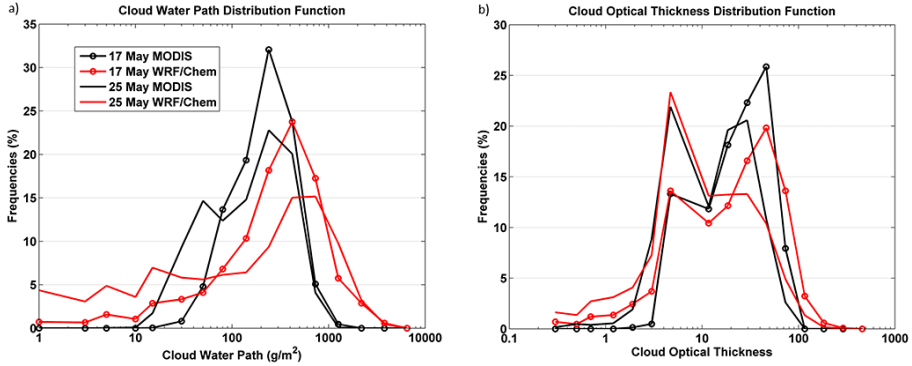

Figure 12. Observed and simulated distribution function of cloud water path **(a)** and cloud optical thickness **(b)** on 17 and 25 May 2008.

GMDD
8, 791–853, 2015

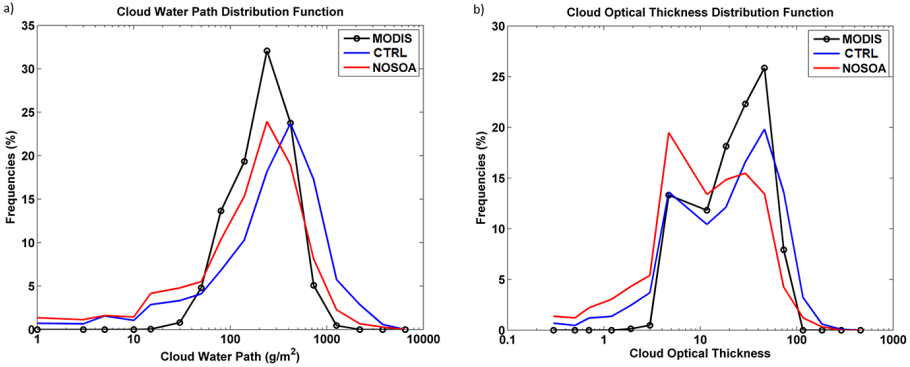

Figure 13. Comparison among the simulated distribution functions of CWP and COT in CTRL (blue) and NOSOA (red) run, and MODIS (black) observations.

GMDD
8, 791–853, 2015

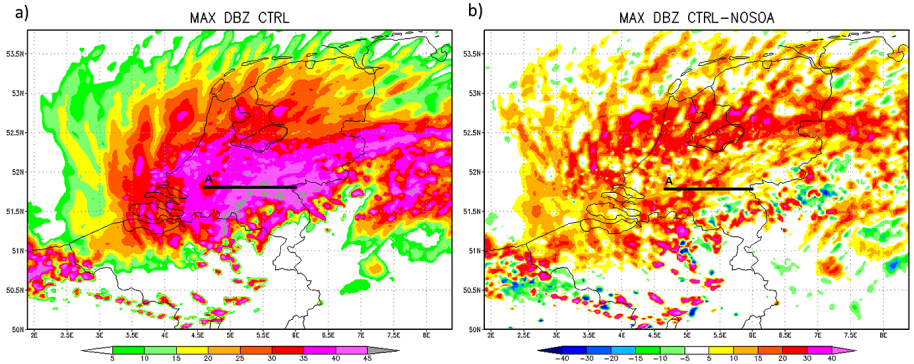

Figure 14. Maximum dbz at 06:00 UTC of 17 May for CTRL run **(a)** and difference of maximum dbz between CTRL and NOSOA simulations **(b)**. The solid black line represents the cross section A of the vertical profiles reported in Fig. 13.

GMDD
8, 791–853, 2015

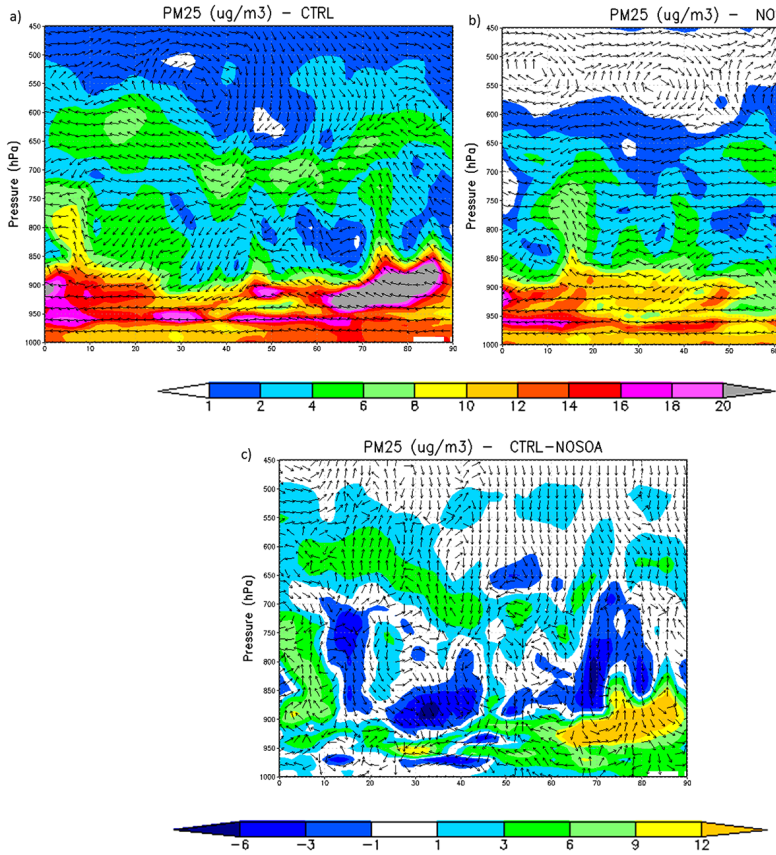

Figure 15. Vertical profile of $PM_{2.5}$ mass (color) and wind (vector) for CTRL run **(a)**, NOSOA run **(b)** and their differences **(c)**. The fields are extracted along the cross section A (see Fig. 12) at 06:00 UTC of 17 May. The *x* axis reports the west–east distance in km along the cross section.

GMDD
8, 791–853, 2015

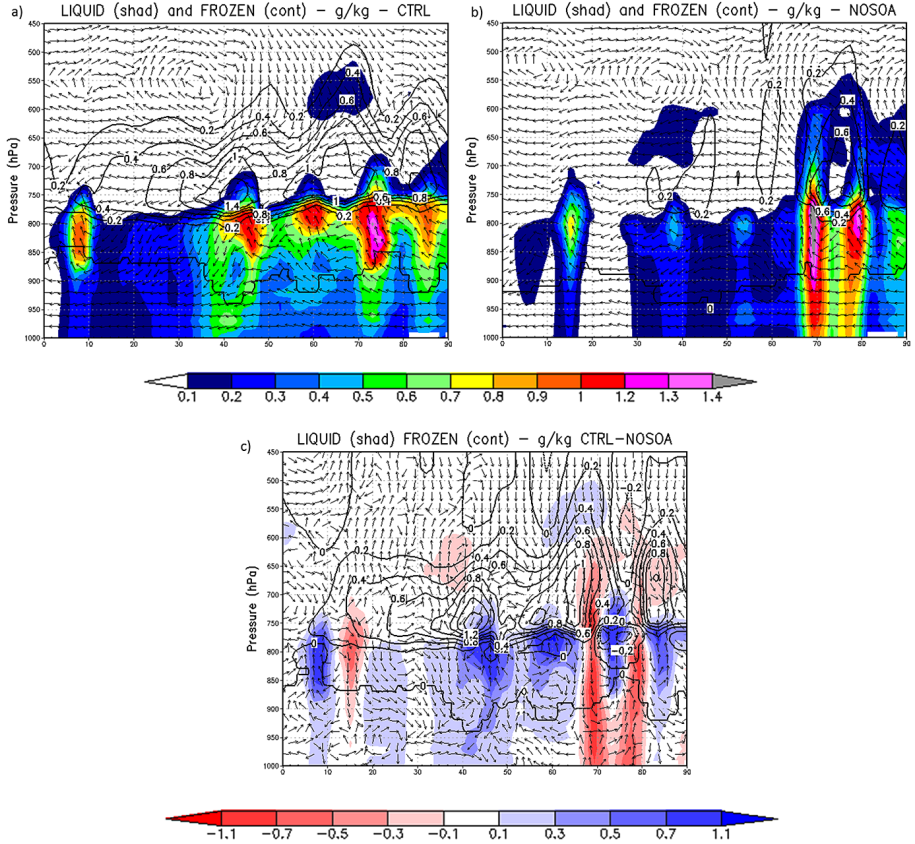

Figure 16. As Fig. 15, but for water (color) and frozen (black contours) hydrometeors.

GMDD
8, 791–853, 2015